Analytical and Simulation Study of Sweep Efficiency in Gas-Injection EOR

Guanqun Yu

To obtain the degree of Master of Science at the Delft University of Technology

To be defended publicly on Friday August 28th, 2015 at 09:30AM.

Student number: 4260872

Project duration: November 1st, 2014 – August 28th, 2015

Thesis committee:

Prof. Dr. W. R. (William) Rossen,	TU Delft, Supervisor.
Prof.Dr.Ir.J.D. Jansen,	TU Delft.
Ir. A.G. (Andre) van Turnhout,	TU Delft.

TU Delft Delft University of Technology

Table of Content

Abstract

WAG (Water-Alternating-Gas injection) is a non-thermal EOR process, which was proposed to improve the volumetric sweep efficiency and consequently the oil recovery during a gas injection project. Though miscible gas injection gives fantastic displacement efficiency due to its miscibility with oil, it usually shows very poor volumetric sweep efficiency due to the high mobility of gas phase. Alternate injection of gas and water significantly reduces the gas relative mobility, and therefore leads to less gas fingering and/ or tonguing of gas. The benefit of water injection can be further improved by replacing cold water with heated water. The idea of co-injecting hot water with miscible gas was originally proposed by Dr. Namani *et al*. (2013). They refer to this method as miscible hot WAG for EOR (in the following content we call it HWAG), where by co-injection of hot water and first-contact-miscible gas, a significant increase in volumetric sweep efficiency for oil (especially for heavy oil) displacement can be achieved. Core-flooding experiments have been done on HWAG and show significant improvements over oil recovery compared to conventional WAG EOR and hot water flood (Namani *et al*, 2013).

Aside from fingering and channeling, gravity segregation is another major effect that leads to the deterioration of sweep efficiency in gas-injection EOR processes. After the injected gas and water travels a certain distance in the reservoir, they completely segregate from each other under gravitational forces. Gas goes to the top of reservoir forming an override zone, and water goes to the bottom forming an under-ride zone. This effect is ineffective because, after gas and water are completely separated, only a thin region at the reservoir top can be swept by gas. And after the gas breakthrough, all the gas injected afterwards escapes from the override zone and becomes wasted. Estimation of the complete segregation distance between gas and water is therefore crucially important for drilling and production plans. Stone (1982) developed an analytical model to predict the gravity segregation process in homogeneous horizontal reservoirs. Namani *et al.*(2012) extended the model for gravity segregation in homogeneous non-horizontal reservoirs. His model, which lacks rigorous mathematical proof, requires examination from extensive study of numerical simulation.

In Chapter one, fractional-flow theory is applied to provide insight into the advantages of HWAG. The fractional-flow method describes the flooding process in 1-D homogeneous reservoirs, which can be applied to a wide range of EOR processes. The method is accurate, when its assumptions are satisfied, in reflecting the saturation, front position and relative mobility of the agents injected, from which an optimal injection strategies can be determined. The fractional-flow method is applied here to conventional WAG EOR, hot water flood and HWAG EOR. Comparing the results of the three methods, the main advantage of hot water injection in HWAG is the reduction of the mobility contrast between the miscible gas bank and the oil bank. By adjusting the fraction of hot water injected, an optimal injection condition can be determined. The control over phase relative mobilities by hot water under optimal condition leads to significantly better sweep efficiency, which gives the improved oil recovery observed in the core-flooding experiments. One major set-back of HWAG may be that of the large amount of hot water required in order to achieve an optimal injection condition. Therefore, the amount of hot water available holds the key to the success of miscible hot WAG.

The main focus of Chapter two is the simulation study of gravity segregation in non-horizontal reservoirs. First, extensive simulations are done to examine the accuracy of Namani's model for the segregation distance in dipping reservoirs. Our result show that the model is doesn't work accurately; the influence of dipping angle over segregation distance needs to be further explored using numerical simulations. Second, it is equally important to understand all the dynamic processes during the process of gravity segregation. These dynamic processes may give us a better understanding about the physics involved, and provide some valuable instructions for drilling & production strategy.

Acknowledgement

My sincere gratitude to my supervisor Prof. Dr. W. R. (William) Rossen. He has been a great tutor on my thesis project, guiding me with unparallel care and patience. His superior level of knowledge and wisdom profoundly inspires me, opening up my mind and illuminating my way forward on scientific research. I would never be able to accomplish as much as I did in this paper without his continuous encouragement and guidance. The experience of working with him is a great treasure to me.

Many thanks to PhD student Alexander (Jinyu) Tang; Msc student Rahul Ranjan Singh, Ahmed Al Auesh, Xiaofei Gan and Fei Chen. They have been most caring and supportive friends. I am more than grateful for their help along the way.

Finally, I want to thank my dearest parents. I would never finish the project without their strong support. They are the best.

Chapter 1-Fractional-flow Analysis of Miscible Hot WAG

Miscible hot WAG is a newly proposed hybrid method for the enhancement of oil recovery. This new technique has not yet been tested in the field; therefore its efficiency for oil production in real life remains unclear to us. However, some fundamental studies have been done to explore its nature.

Core flooding experiments with Pentane showed considerably higher recovery factor achieved by miscible hot WAG compared to those of cold WAG and hot water flood (Namani *et al*, 2013). The fractional-flow method, or the method of characteristics (MOC), is extensively used in this chapter to provide insights into this technique. At first, three scenarios for miscible hot WAG are studied to examine the effects of water fraction injected. Afterwards, fractional-flow model of cold WAG and hot water flood are both examined and compared to the miscible hot WAG. This comparison was also using Namani's experiments for both slightly heavy oil and heavy oil components to analyze their influence over oil recovery. Finally, a sensitivity analysis is done to examine the effects of different parameters (e.g. the impact of porosity over heat loss).

The fractional-flow approach leads to the following conclusions. Propagating a thermal front ahead of the miscible front reduces the mobility ratio at the miscible front. This would reduce fingering and channeling and improve sweep efficiency. If the thermal front trails the miscible front, it plays no role in oil displacement. Because most of the heat in the injected hot water is consumed heating the formation, a large volume of hot water must accompany a given volume of solvent. We derive a condition for an optimal WAG ratio, in the sense that the thermal front stays just in front of the miscible front, based on formation and fluid properties. We show how this optimal WAG ratio changes as a function of formation properties. Because so much hot water must be injected along with solvent, the process would ideally suited to a project where the possible rate of solvent injection is limited (e.g., a project with solvent supplied by an industrial process with limited output). Then the additional hot water can be injected without slowing the overall process.

Our approach assumes that the solvent is miscible with the crude oil at both the initial temperature of the reservoir and at the temperature of the hot-water flood.

1.1. Introduction

The idea of miscible hot WAG was originally put forward as a hybrid EOR method for heavy oil as well as slightly heavy oil production. The idea behind it is to combine the competitive advantages of hot water flood and miscible, WAG (water alternating gas injection).. Though the advantage of applying this technique to light oil production is not yet fully understood, its significant improvements over heavy oil recovery have been studied by core flooding experiments (Namani *et al*, 2013).

Conventionally, either solvent flooding or thermal flooding has been applied individually to enhance heavy oil recovery. Solvent floods, on the one hand, usually result in (almost) zero residual oil saturation and thus exhibit excellent displacement efficiency. However, they mostly exhibit very poor sweep efficiency with serious effects of gravity override, gas channeling and viscous fingering, due to the low gas viscosity and density (Lake, 1989). Both light oil and (especially) heavy oil displacement suffer from the poor sweep by gas. Therefore, water-alternating-gas injection (WAG) was proposed to enhance the sweep of gas phase. The WAG method, on the one hand, partially hampers gravity override effect, particularly when solvent is only injected from the lower part of the perforation interval while water is injected from the upper part. On the other hand, this method has proven to be very efficient when it comes to killing gas fingers. When gas fingers start to grow, the water injected tends to move forward through the easy path into the fingers and fill them with water. The gas behind it then tends to go sideways around it, and the fingers thus collapse.

Thermal methods, particularly steam injection and steam soak, are highly effective in terms of reducing oil viscosity. Steam has a relatively higher efficiency of heat injection than hot water floods, due to the simple fact that steam carries much more heat (latent heat) into the surroundings before it cools off than hot water of the same temperature. Steam, meanwhile, reduces the IFT (interfacial tension) and vaporizes the light oil components. However, steam

injection suffers from the poor sweep efficiency. Hence SAGD (surfactant assisted gravity drainage) was proposed to resolve the issue of poor sweep by taking advantage of gravitational force.

Experimental studies already showed considerably higher recovery factor achieved by miscible hot WAG for both heavy oil and slightly heavy oil components (Namani *et al*, 2013). This technique has the following characteristics:

1. Hot water has a better sweep and is much cheaper than steam. Its low displacement efficiency could be compensated by mixing with miscible solvent. This character shares similarity with that of adding miscible solvent to a SAGD process.

2. Being assisted by hot water, miscible solvent flood now has even better sweep efficiency compared to that of the cold WAG due to thelower mobility contrast between oil phase and gas phase.

3. In conclusion, the hybrid technology lowers the production cost, while maintaining the recovery efficiency compared to other conventional flooding methods.

4. One important issue of combining miscible solvent with thermal flood is that of the reduced miscibility (if we are injecting CO_2) at high temperatures. Thus serious considerations ought to be taken over controlling the temperature level of injected thermal agent(s) (hot water in this case, in other cases there are examples when solvent are added in SAGD process) to maintain the miscibility of solvent(s).

1.2. Fractional-flow method

Fractional-flow theory has been applied to analyze various traditional flooding processes as well as EOR methods since the 1940's (Buckley & Leverret, 1941). The fractional flow method has proven to be a very accurate instrument to simulate miscible and immiscible flooding processes. Assumptions include incompressible phases; Newtonian mobility; 1D horizontal displacement; absence of gravitational force; absence of dispersion effects, capillary gradient and viscous fingering; immediate attainment of local steady state (E. Ashoori, 2009). In this article, the fractional-flow method is primarily applied to analyze the various scenarios in a hot miscible WAG flood.

The fractional-flow method originated from the method of characteristics (MOC), which is one of the many ways to solve hyperbolic PDEs. From the law of conservation of mass, the phase saturation distribution in both spatial and temporal dimensions could be constructed, which is in the form of a hyperbolic partial differential equation (Eq. [1.1]). The water conservation of mass equation the with source term neglected yields:

$$\frac{\partial S_w}{\partial t} + \langle \frac{u_t}{\varphi} \frac{df_w}{dS_w}\Big|_{S_w} \rangle \frac{\partial f_w}{\partial x} = 0 \qquad \textbf{Eq. [1.1]}$$

The specific velocity $\frac{u_t}{\varphi}\frac{df_w}{dS_w}\Big|_{S_w}$ of a characteristic S_w is determined by the derivative $\frac{df_w}{dS_w}$, with constant total injection rate u_t and constant φ by assuming incompressible homogeneous matrix. Writing the specific velocity in dimensionless form(Eq. [1.2]):

$$v_w = \frac{\Delta x_D}{\Delta t_D} = \frac{\Delta x/L}{u_t \Delta t/\varphi L} = \frac{df_w}{dS_w}\Big|_{S_w} \qquad \textbf{Eq. [1.2]}$$

Solving this problem involves two main steps. The first step is to determine the initial condition 'I' and injected condition 'J' on the fractional-flow curve(s). The second step is to find a composition route from J to I with monotonously increasing slope, which guarantees the physical consistency of the solution. The shock velocity must satisfy(Eq. [1.3]):

$$v_{w,shock} = \frac{\Delta f_w}{\Delta S_w} = \frac{df_w}{dS_w} = v_{w,jump} \qquad \textbf{Eq. [1.3]}$$

In the fundamental cases of immiscible two phase flow, there is only one fractional flow curve (oil/cold water) involved. In EOR processes, however, multiple fractional flow curves are required in the analysis, and jumps between the curves are required to describe the shocks formed by injected agents.

All the scenarios below are discussed in the context of 1D flow in porous media. In a 2D or 3D displacement, however, fingering and channeling can reduce sweep efficiency. These processes depend on total relative mobility (Eq. [1.4]).

$$\lambda_{rt} = \sum_{\alpha=1}^{n} \frac{k_{r\alpha}}{\mu_{\alpha}} \qquad \textbf{Eq. [1.4]}$$

A bank of fluid with higher relative mobility will tend to finger through those with lower mobility. This effect is not shown in the 1D solution, but still the mobility of each bank can be identified on all the saturation profiles as a reminder of its possible influence on multiple-dimension flow.

1.2.1. Fractional-flow method of WAG

In cold miscible WAG, when FCM (first contact miscible) solvent (i.e.CO_2) is alternatively injected with cold water (in fractional flow analysis water and solvent are approximated as being co-injected) to displace residual oil, there are two fractional-flow curves involved, which are the cold oil-water and the cold gas-water curves. The initial condition 'I' lies on cold oil-water curve, while the injecting condition 'J' is on the cold gas-water curve. Therefore there must be a jump on the composition route from the oil-water curve to the gas-water curve, which represents the miscible agent(s) front. A mass balance applies at the jump for both water and solvent (Figure 1.1). Ahead (downstream) of the miscible front, there is two-phase flow of oil bank and cold water; behind (upstream of) the front, the residual oil has been completely displaced by FCM gas, and thus there is two-phase flow of cold gas and water.

A mass balance on water at the miscible front gives

$$\Delta x(A\varphi S_w^+ - A\varphi S_w^-) = \Delta t(Au_t f_w^+ - Au_t f_w^-) \qquad \textbf{Eq. [1.5]}$$

where '+' and '-' indicate upstream and downstream states, respectively. The specific velocity of water at miscible front is given by

$$\frac{\Delta x}{\Delta t} = \frac{u_t}{\varphi}\left(\frac{f_w^+ - f_w^-}{S_w^+ - S_w^-}\right) \qquad \textbf{Eq. [1.6]}$$

Written in dimensionless form, this gives

$$v_{w,shock} = \frac{\Delta x_D}{\Delta t_D} = \frac{f_w^+ - f_w^-}{S_w^+ - S_w^-} \qquad \textbf{Eq. [1.7]}$$

Upstream of the miscible front gas fractional flow is $(1 - f_w^+)$; and downstream of the miscible front there is oil instead of gas: $S_g^- = 0$. A mass balance on gas at the miscible front thus gives:

$$\Delta x[A\varphi(1 - S_w^+) - 0] = \Delta t[Au_t(1 - f_w^+) - 0] \qquad \textbf{Eq. [1.8]}$$

The specific velocity of gas front must satisfy

$$v_{g,shock} = \frac{\Delta x_D}{\Delta t_D} = \frac{1 - f_w^+}{1 - S_w^+} \qquad \textbf{Eq. [1.9]}$$

The conditions for the miscible front are thus determined by

$$v_{g,shock} = \frac{f_w^+ - 1}{S_w^+ - 1} = \frac{f_w^+ - f_w^-}{S_w^+ - S_w^-} = v_{w,shock} \qquad \textbf{Eq. [1.10]}$$

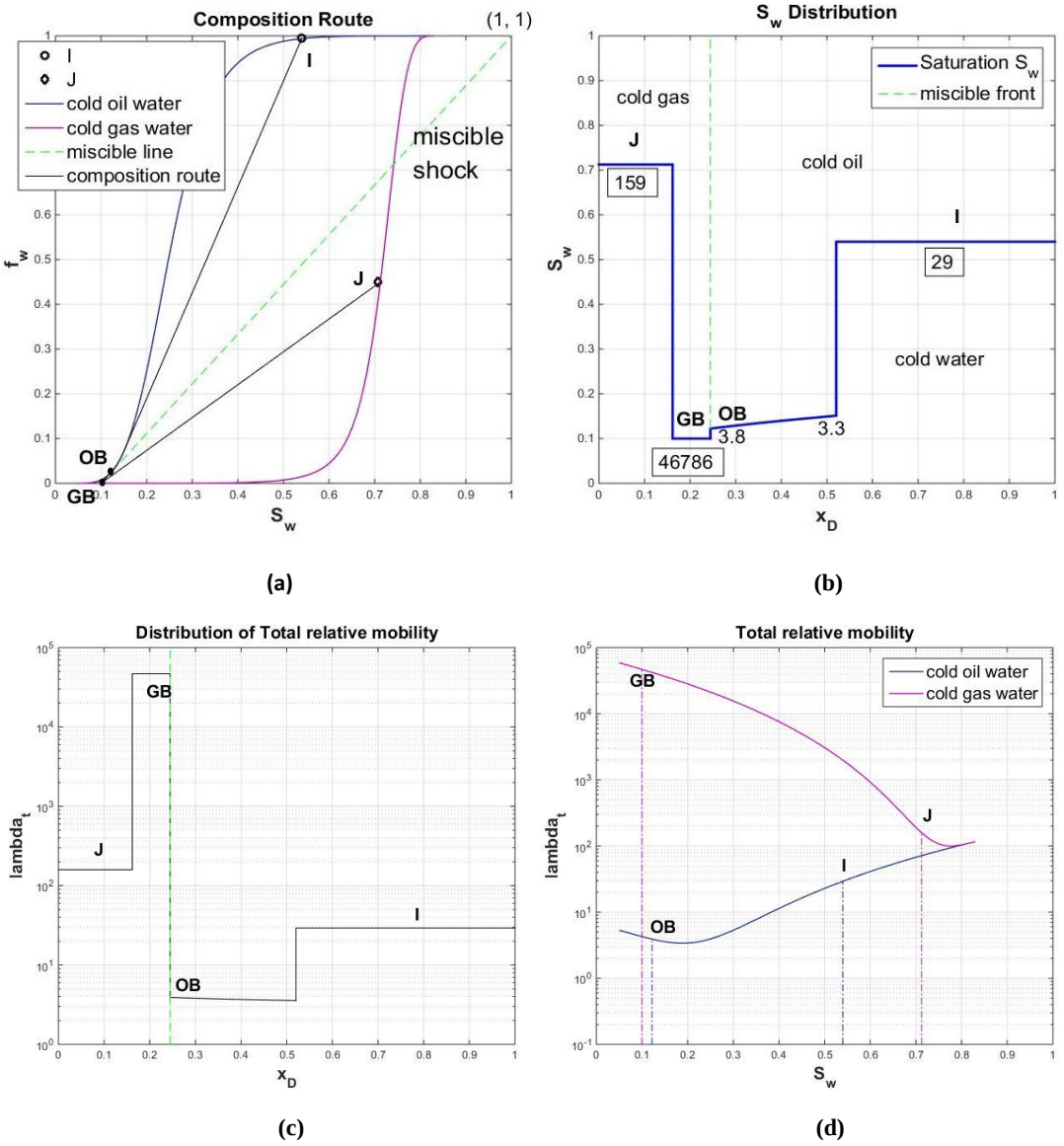

Figure 1.1. Displacement of slightly heavy oil by Pentane at an initial saturation of $S_{wi} = 0.54$ by a mixture of cold water and a gas that is first-contact miscible with oil. Reservoir temperature is assumed to be 21.9℃, consistent with the laboratory conditions (Namani *et al*, 2013). (a) Solution on fractional-flow plot. $f_w = 0.45$ at J. (b) Saturation profile at $t_D = 0.22$. Numbers are total relative mobility, in $(\text{Pa s})^{-1}$. In this and similar figures, boxed values apply to a whole region of constant state. Unboxed values apply to the leading and trailing edge of a spreading wave. (c) Total relative mobility distribution. (d) Total relative mobility of cold WAG as function of water saturation S_w.

Therefore the miscible shock is represented by a line passing through point (1,1), the upstream (gas-water) fractional-flow curve and downstream (oil-water) fractional-flow curves at the at the saturations upstream and downstream of the shock.

According to the given initial conditions and rock-fluid properties, the composition route is uniquely determined and shown in figure 1.1. There is first a cold water shock from initial condition 'I' to 'OB' (oil bank), then followed by a shock from 'OB' to 'GB' (gas bank). At last there is a jump from 'GB' to injection condition 'J'.

1.2.2. Fractional-flow method for hot-water flood

When thermal agent (hot water) is injected into the system, both an energy balance and a mass balance apply. To apply an energy balance within fractional-flow theory, instantaneous achievement of thermal equilibrium is assumed. An energy balance analysis at the hot-water front defines the condition for thermal-front velocity.

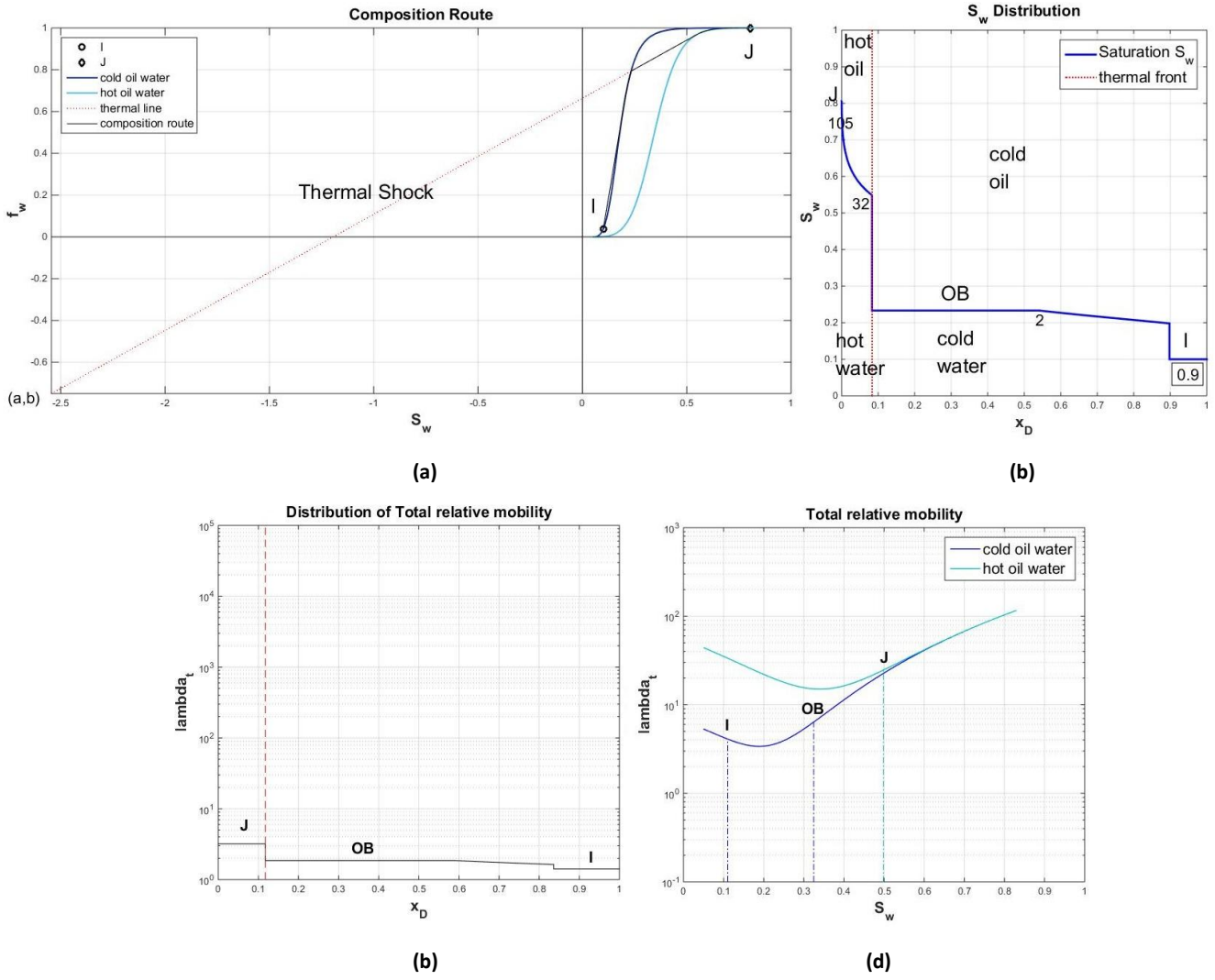

Figure 1.2. Displacement of slightly heavy oil at an initial saturation of $S_{wi} = 0.1$ by hot water of 100 ℃. Reservoir temperature is assumed to be 21.9℃, consistent with the laboratory conditions (Namani *et al*, 2013). (a) Solution on fractional-flow plot. $f_w = 1.0$ at J. (b) Saturation profile at $t_D = 0.15$. (c) Total relative mobility distribution. (d) Total relative mobility of hot water flood as function of water saturation S_w.

Writing the energy equation in the fractional flow form yields (Lake, 1989)

$$\left(M_{Tw}S_w + M_{To}S_o + \frac{1-\varphi}{\varphi}M_{Ts}\right)\frac{\partial T}{\partial t_D} + (M_{Tw}f_w + M_{To}f_o)\frac{\partial T}{\partial x_D} = 0 \qquad \textbf{Eq. [1.11]}$$

M_{Tw}, M_{To} and M_{Ts} are the volumetric heat capacities for water, oil and solid (rock matrix). From this equation, the specific velocity of thermal shock must satisfy

$$v_T = \frac{\Delta x_D}{\Delta t_D} = \frac{M_{Tw}f_w + M_{To}f_o}{M_{Tw}S_w + M_{To}S_o + \frac{1-\varphi}{\varphi}M_{Ts}} = \frac{f_w - \frac{M_{To}}{M_{To}-M_{Tw}}}{S_w - \frac{M_{To}+\frac{1-\varphi}{\varphi}M_{Ts}}{M_{To}-M_{Tw}}} \equiv \frac{f_w - b}{S_w - a} \qquad \textbf{Eq. [1.12]}$$

A mass balance on water at the thermal front gives:

$$v_{w,shock} = \frac{f_w^+ - f_w^-}{S_w^+ - S_w^-} \qquad \textbf{Eq. [1.13]}$$

The thermal front velocity has to satisfy both conditions. This is represented by a line passing through point (a, b), as well as the upstream (hot-water) fractional-flow curve and the downstream (cold-water) fractional-flow curve. Figure 2.2 illustrates the solution on fractional-flow plots of slightly heavy oil displaced by hot water of $100℃$.

1.2.3. Fractional-flow method for miscible hot WAG

Miscible hot WAG is a method that combines both cold WAG and hot-water flood. Therefore, fractional-flow analysis for this technique involves both a thermal (hot water) shock and miscible shock. There are altogether four fractional-flow curves, which are the cold oil-water fractional curve, the hot oil-water fractional curve, the hot gas-water fractional curve and the cold gas-water fractional curve.

There are two scenarios for miscible hot WAG:

(1) The thermal front has a higher specific velocity than miscible front; when large water fraction is injected.

(2) The thermal front has a slower velocity than miscible front, when the water fraction injected is lower than a certain threshold.

When the thermal front travels faster than the miscible front, the thermal shock is represented by the jump from the cold oil-water curve to the hot oil-water curve; the miscible front, on the other hand, jumps from the hot oil-water curve to the hot gas-water curve. In the opposite case, the thermal front jumps from the cold gas-water fractional-flow curve to the hot gas-water curve. The miscible front then jumps from the cold oil-water fractional-flow curve to cold gas-water curve. If the two fronts keep the same velocity, there would be one mixed jump from the cold oil-water curve to the hot gas-water curve. Three examples which illustrate these conditions in detail are given in the following text.

There exists a threshold value for the water fraction injected, which in this chapter is denoted as f_w^*. This value provides a boundary which separates an efficient thermal flood (when $f_w \geq f_w^*$) with an inefficient thermal flood. f_w^* is determined by the intersection of a line passing through points (a, b) and (1, 1) with the hot gas-water fractional-flow curve (Eq.1.14).

$$[(S_w^* - 1) * A + 1] * (1 + M) - 1 = 0 \qquad \textbf{Eq. [1.14-a]}$$

$$f_w^* = \frac{\left({}^{a_1}/_{a_3}\right)^{cw}}{\left({}^{a_1}/_{a_3}\right)^{cw} + {}^{1}/_{M} \cdot \left({}^{a_2}/_{a_3}\right)^{cg}} \qquad \textbf{Eq. [1.14-b]}$$

- $A = {}^{(1-b)}/_{(1-a)}$
- $M = \frac{\lambda_w}{\lambda_g} = \frac{k_{rw}}{k_{rg}} \frac{\mu_g}{\mu_w}$
- $a_1 = S_w - S_{wr}$
- $a_2 = 1 - S_w - S_{wr}$
- $a_3 = 1 - S_{wr} - S_{gr}$

Eq. [1.14-a] gives the water saturation corresponding to the threshold water fraction, and f_w^* can be computed according to Eq. [1.14-b]. Refer to Appendix A for parameter values.

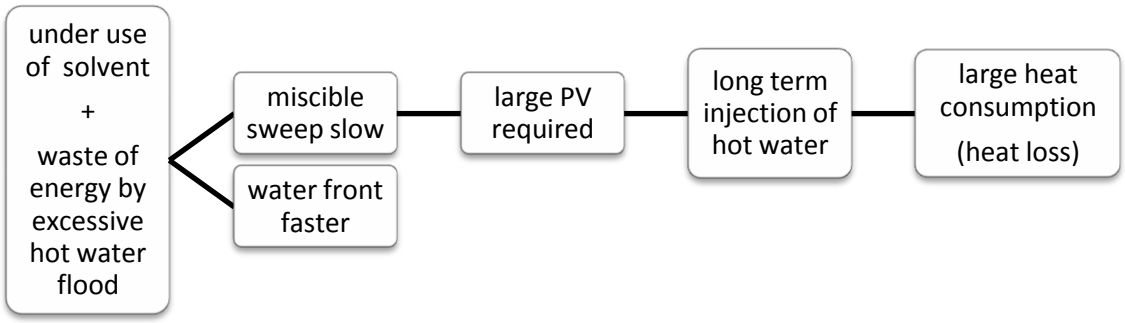

Figure 1.3. The negative effects brought about by excessive injection of hot water.

When the injected water fraction is much larger than f_w^*, the thermal front travels much faster than the miscible front, in which case the injected miscible agent is being under-used. The excessively injected hot water will be running ahead of the solvent injected and result in heat loss to the formation. The gas front moves very slowly, and it takes a very long time of overall injection before the solvent sweeps the entire reservoir (Figure 1.3). Figure 1.4 illustrates the solution on the fractional-flow plots.

In cases when f_w injected is smaller than f_w^*, the miscible front will move ahead of the thermal front. In such cases the process becomes conventional WAG displacement, when oil is being displaced by cold miscible gas, and hot water followings behind but it has no effect on the displacement (Figure 1.5). Figure 1.6 illustrates the fractional-flow solution.

The optimal water fraction (Figure 1.7) for miscible hot WAG maintains the hot water (thermal) front slightly ahead of the gas (miscible) front; the hot water pre-heats the oil before the arrival of miscible gas. This condition represents the best scenario for mobility control; the mobility contrast between the hot gas and the hot oil ahead of it is reduced. It also suggests the proper use of hot water and solvent, when neither one of them is being excessively injected. Therefore, keeping the hot water bank slightly but not too much ahead of the gas bank will lead to the reduction of energy consumption, which in turn lowers the expenditure. Figure 1.7 illustrates the optimal condition for miscible hot WAG, which guarantees the best efficiency of this method.

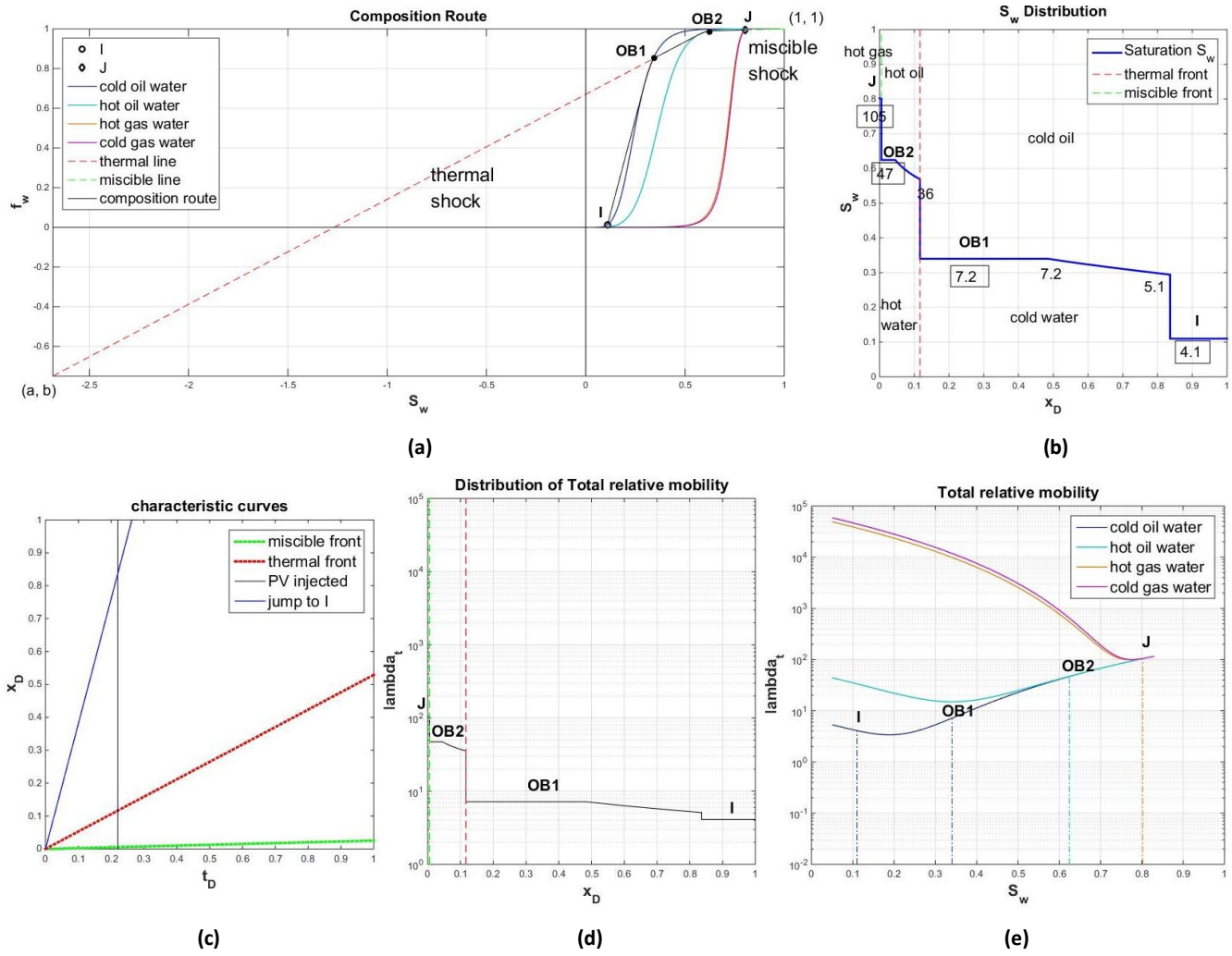

Figure 1.4. Displacement of oil by Pentane at an initial water saturation at I of 0.1 by a mixture of hot water of $100℃$ and a gas that is first-contact miscible with oil. Injected hot-water fraction $f_w \gg f_w^*$. (a) Solution on fractional-flow plot for f_w^* at $J = 0.995$. (b) Saturation profile at $t_D = 0.22$. (c) Characteristic curves. (d) Total relative-mobility distribution. (e) Total relative mobility of miscible hot WAG as function of S_w.

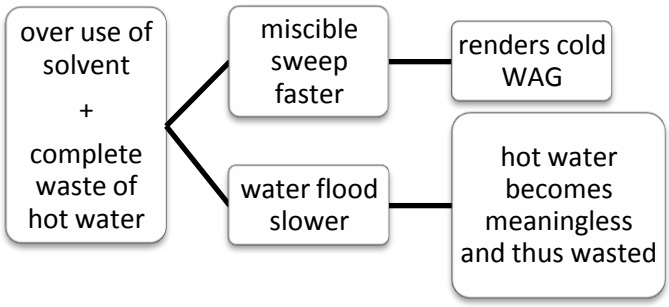

Figure 1.5. The negative effects brought about by excessive solvent injection.

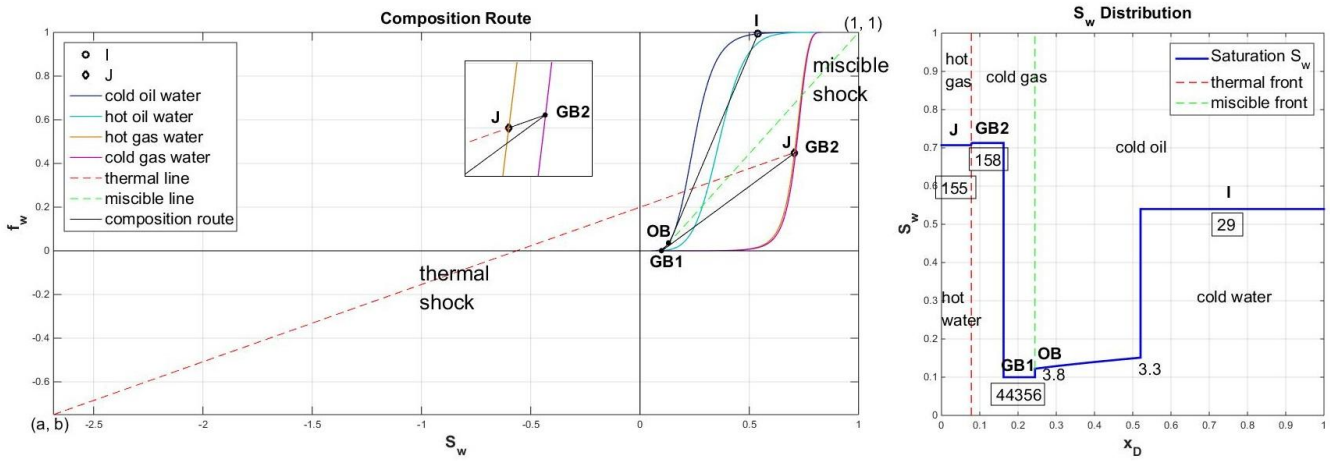

(a) **(b)**

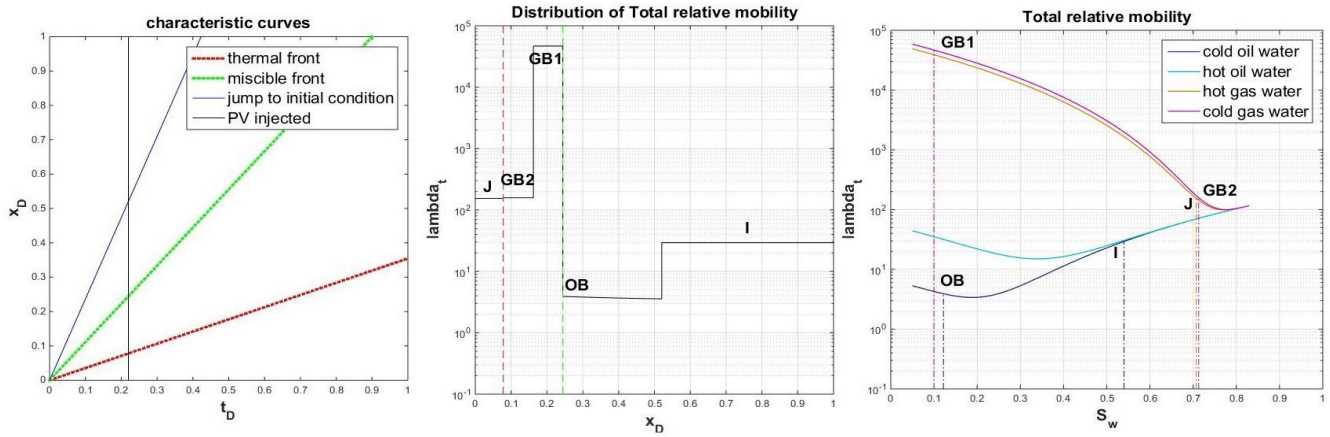

(c) **(d)** **(e)**

Figure 1.6. Displacement of slightly heavy oil at an initial water saturation at I of 0.54 by a mixture of hot water of 100 ℃ and a gas that is first-contact miscible with oil. Reservoir temperature is assumed to be 21.9℃, consistent with the laboratory conditions (Namani *et al*, 2013). In this case, the miscible shock travels faster than the thermal shock: $f_w \ll f_w^*$. (a) Solution on fractional-flow plot. $f_w = 0.45$ at J. b) Saturation profile at $t_D = 0.22$. (c) Characteristic curves. (d) Total relative-mobility distribution. (e) Total relative mobility of miscible hot WAG as function of water saturation S_w.

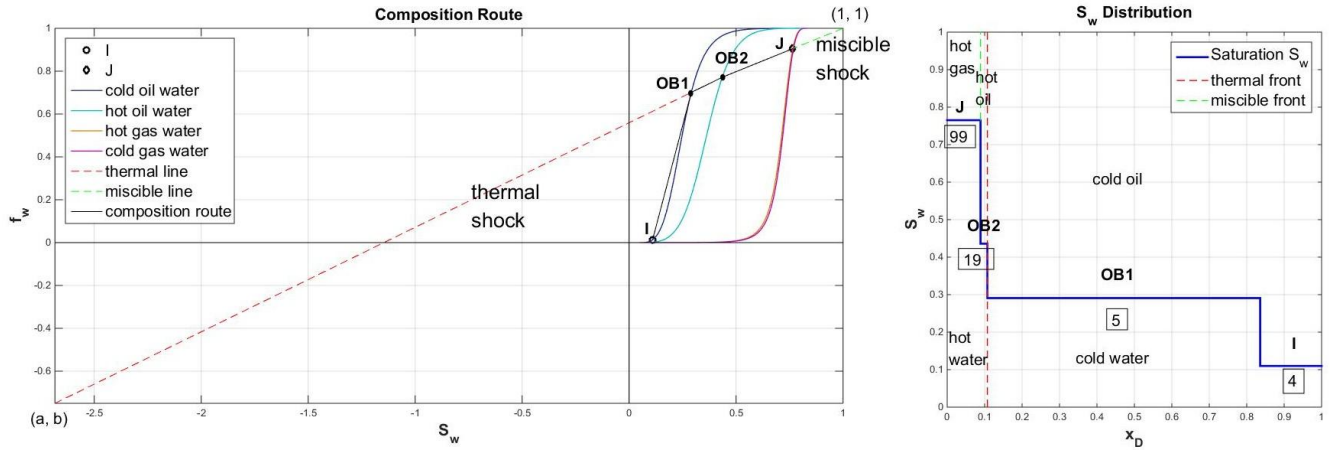

(a) **(b)**

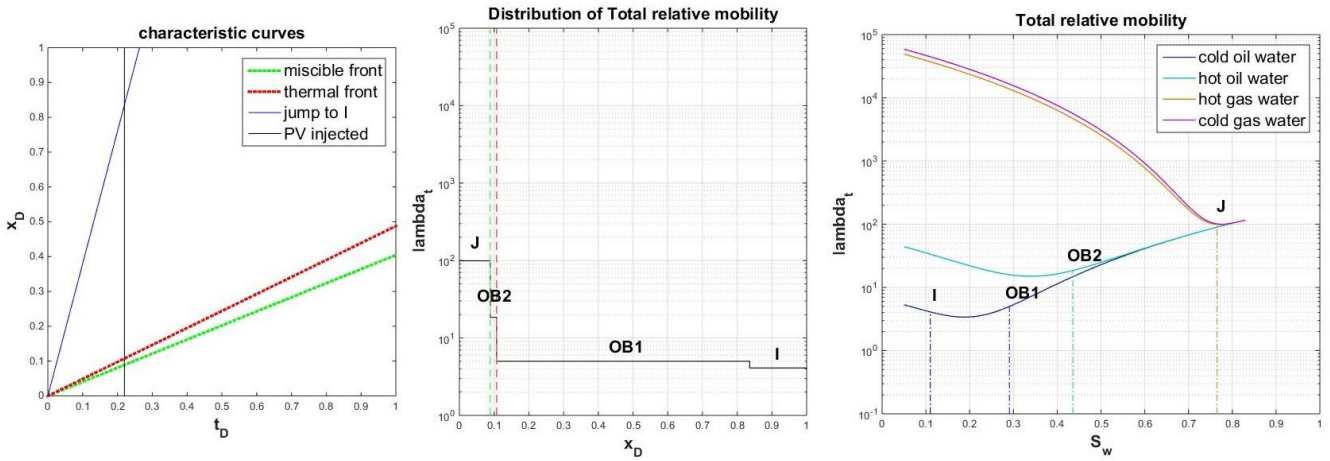

(c) **(d)** **(e)**

Figure 1.7. Displacement of slightly heavy oil at an initial water saturation of $I = 0.1$ by a mixture of hot water of $100℃$ and a gas that is first-contact miscible with oil. Reservoir temperature is assumed to be $21.9℃$, consistent with the laboratory conditions (Namani *et al*, 2013). In this case, we have the optimal condition for miscible hot WAG: the thermal front is just ahead of the miscible front $f_w > f_w^*$. (a) Solution on fractional-flow plot. $J = 0.905$. (b) Saturation profile at $t_D = 0.22$. (c) Characteristic curves. (d) Total relative mobility distribution. (e) Total relative mobility of miscible hot WAG as function of water saturation S_w.

1.3. Hot WAG, Cold WAG and Hot Water flood for slightly heavy oil

Core-flooding experiments on heavy oil components (Namani *et al*, 2013) have shown great potential for the application of miscible hot WAG, which achieved considerably higher recovery factor (RF) than those of cold WAG and hot-water flood. However, the fluid-flow mechanism, which is the reason for higher RF of this technique, is not yet fully understood. Therefore, fractional-flow analysis upon all three methods in comparison with one another needs to be done for sake of better understanding. Figure 1.8 (a)-(f) provides an illustration of the mobility distribution for miscible hot WAG compared to that of cold-water WAG.

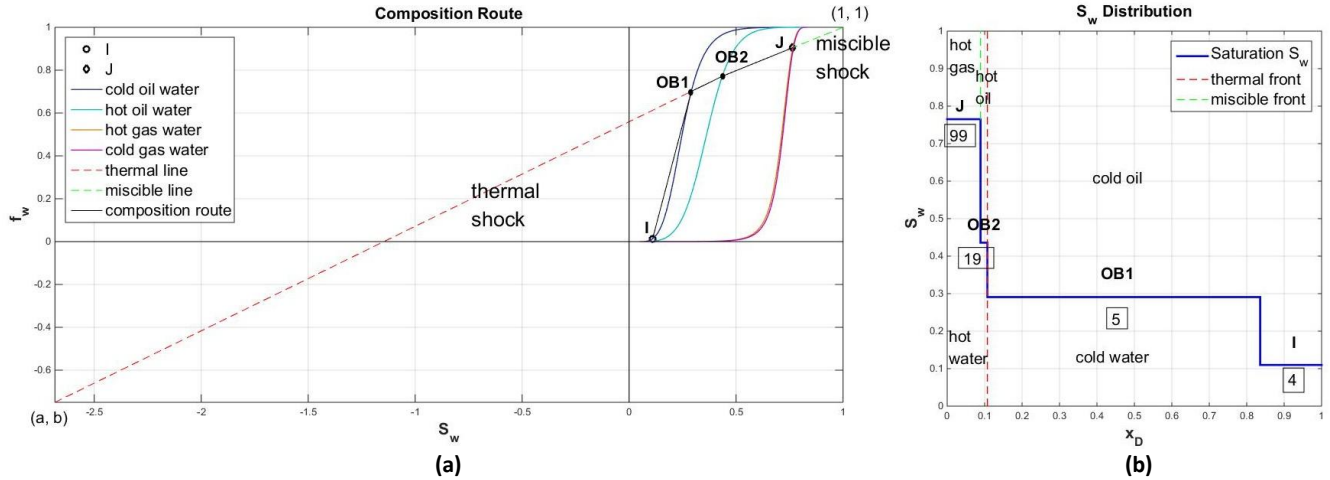

(a) **(b)**

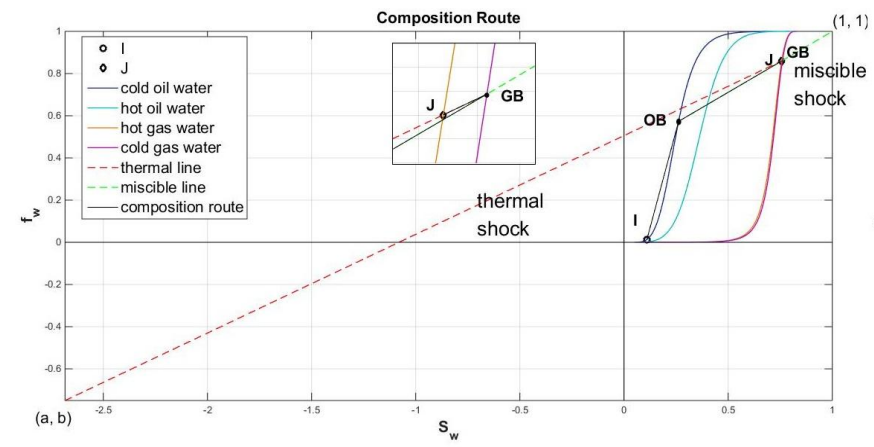

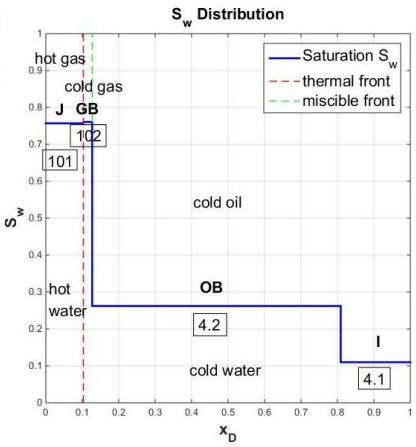

(c) (d)

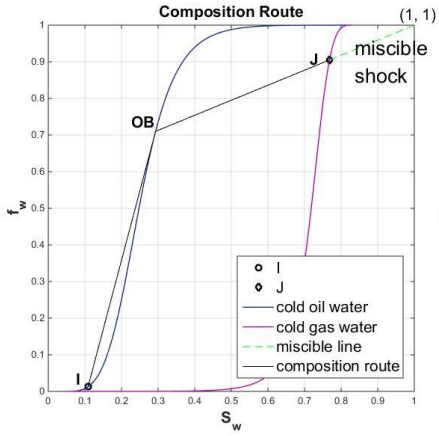

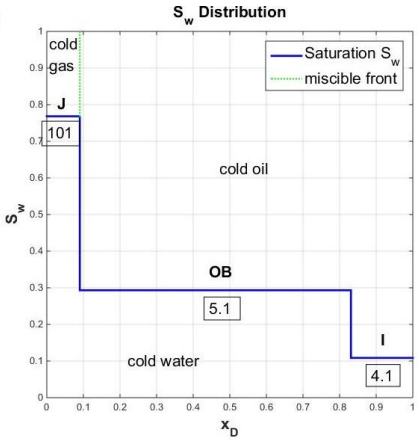

(e) (f)

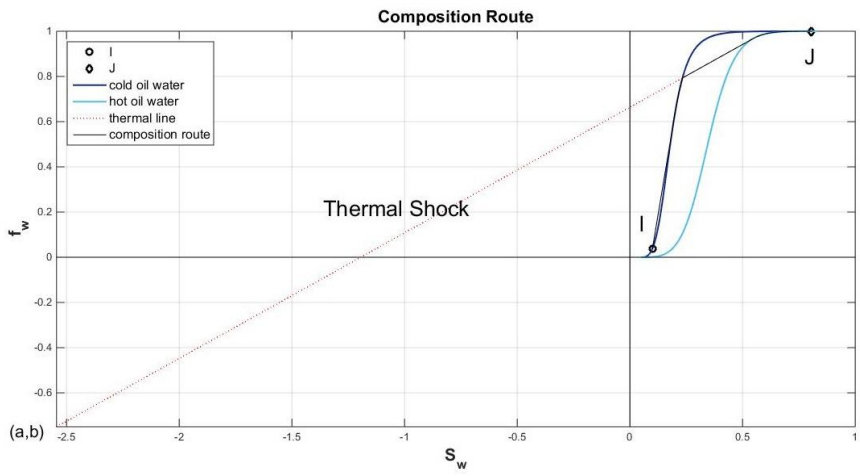

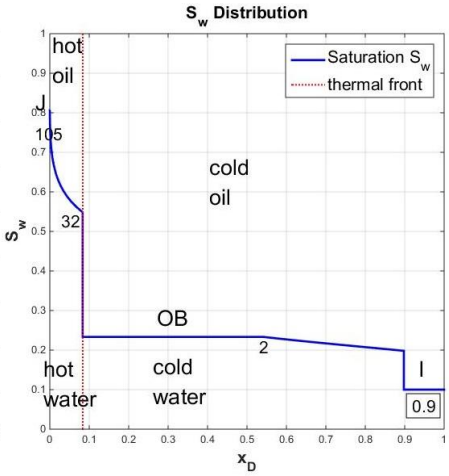

(g) (h)

Figure 1.8. Solution on fractional-flow plot. (b) Saturation profile for miscible hot WAG. S_w at J is 0.905, $t_D = 0.22$. Mobility ratio $\lambda_g/\lambda_o = 99/19 = 5.21$. (d) Saturation profile for miscible hot WAG. S_w at J is 0.86, $t_D = 0.22$. Mobility ratio $\lambda_g/\lambda_o = 102/4.2 = 24.29$. (f) Saturation profile for cold WAG.S_w at J is 0.905, $t_D = 0.22$. Mobility ratio $\lambda_g/\lambda_o = 101/5.1 = 19.8$. (h) Saturation profile for hot water flood. S_w at J is 0.905, $t_D = 0.22$. Mobility ratio $\lambda_g/\lambda_o = 24.61/6.38 = 3.86$.

In 1D flow analysis, both hot WAG and cold WAG can achieve a residual oil saturation of zero, or an ultimate recovery factor of one. Therefore, the advantage(s) of hot WAG must have to do with the control over relative mobility, which largely determines the sweep efficiency of a flooding process. When optimal water fraction is injected in miscible hot WAG, the mobility ratio between oil and gas is approximately $\lambda_g/\lambda_o = 99.5/20 = 4.98$.If, however, the gas front travels faster than the hot water front, or in case of cold WAG with the same water fraction injected, there is a considerable increase in the mobility ratio (102/4.2=24.29 and 101/5.1=19.8) compared to that of the optimal condition of hot WAG. This result shows that miscible hot WAG has a more stable sweep than cold WAG. Figure 1.8 (a)-(b) and (g)-(h) compares the optimal condition of miscible hot WAG to hot-water flood. The major difference between the two methods is the miscible gas injection, which is the key reason why miscible hot WAG achieves much better oil recoveries (almost twice as much according to lab results) than hot-water flood does.

1.4. Miscible hot WAG with lighter oil

From the favorable outcome of both lab experiments and fractional-flow analysis, the effect of miscible hot WAG over heavy oil recovery appears promising. Is it as promising a technique for conventional light oil recovery as for heavy oil? Fractional-flow analysis could provide some insights into this question.

Figure 1.9 (a)-(c) gives the saturation profiles for miscible hot WAG for heavy oil, slightly heavy oil and light oil displacements, Figure 1.9 (d)-(f) give the saturation profiles for cold WAG for heavy oil, slightly heavy oil and light oil displacements. From the figures, the mobility ratio of each method can be read (Table 1.1). This result may suggest that for light oil production, the control over relative mobility by miscible hot WAG is no longer a major competitive advantage compared to conventional cold WAG.

λ_g/λ_o	Heavy oil	Slightly heavy oil	Light oil
Hot WAG	6.19	5.21	1.77
Cold WAG	12312	19.80	3.22

Table 1.1. Relative mobility ratios for miscible hot WAG and cold WAG.

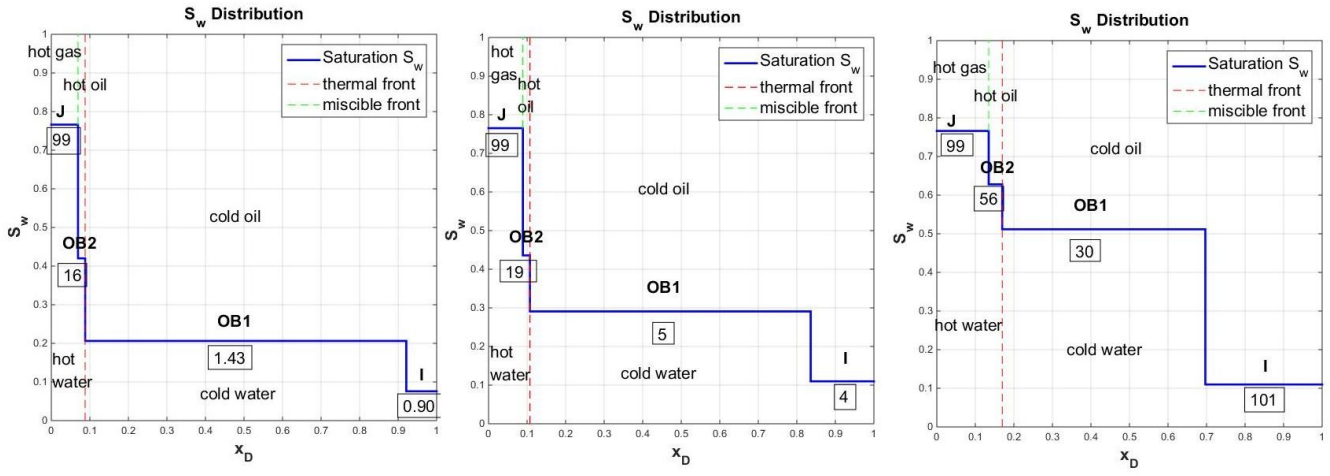

(a) **(b)** **(c)**

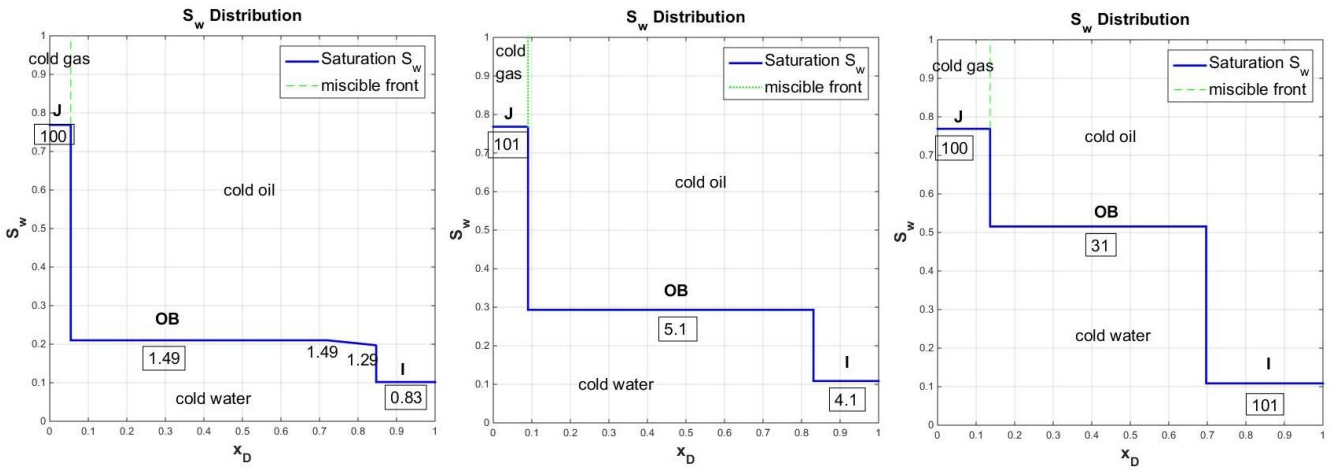

(d) **(e)** **(f)**

Figure 1.9. Saturation profile of miscible hot WAG for (a) Heavy oil. $f_w = 0.905$ at J, $t_D = 0.18$. (b) Slightly heavy oil. $f_w = 0.905$ at J, $t_D = 0.22$. (c) Light oil. $f_w = 0.905$ at J, $t_D = 0.35$. And saturation profile of cold WAG for (d) Heavy oil. $f_w = 0.905$ at J, $t_D = 0.14$. (e) Slightly heavy oil. $f_w = 0.905$ at J, $t_D = 0.22$. (f) Light oil. $f_{wj} = 0.91$ at J, $t_D = 0.15$. $f_w = 0.905$ at J, $t_D = 0.35$.

For heavy oil and slightly heavy oil (Table 1.1), the improvement in mobility control made by miscible hot WAG is significant, which makes this technique competitive with cold WAG. However, the improvement in mobility control of hot WAG for light oil is not as significant. To understand the process completely, of course, one would to take into account some other complexities in real reservoirs (i.e. fingering, channeling, gravity override, type of formation rock, heterogeneity of reservoir etc); otherwise it will be very difficult to determine which method is the better option.

During thermal EOR, most of the heat carried by thermal agents is lost to the formation containing the oil, while a fraction is used to heat the hydrocarbons. Therefore, the heat capacity as well as the porosity of the reservoir formation plays an important role in the efficiency of thermal EOR.

Figure 1.10 (a)-(f) illustrates the effects of formation heat capacity and reservoir porosity over thermal front velocity. The outcomes suggest that miscible hot WAG applies better in a reservoir with lower heat capacity and higher porosity.

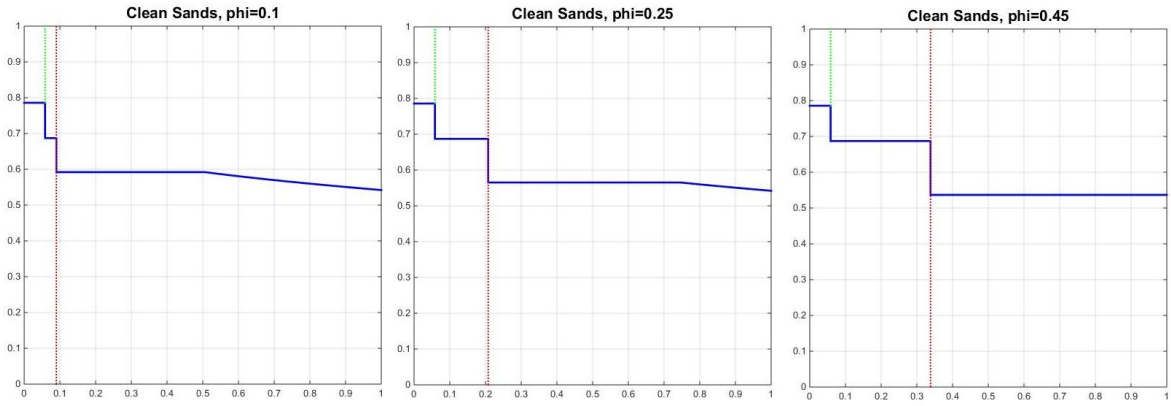

(a) **(b)** **(c)**

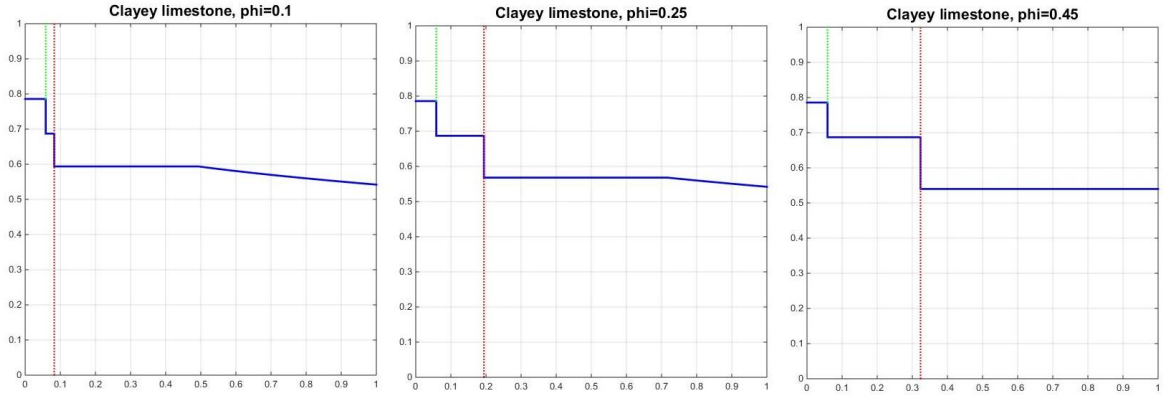

(d) **(e)** **(f)**

Figure 1.10. Saturation profile of miscible hot WAG for (a)(b)(c) Clean Sandstone (d)(e)(f) Clayey Limestone with porosity ranging from 0.1 to 0.45. $f_w = 0.975$ at J, $t_D = 0.5$. (a)-(d) $\varphi = 0.1$. (b)-(e) $\varphi = 0.25$. (d)-(f) $\varphi = 0.45$.

	$\varphi = 0.1$			$\varphi = 0.25$			$\varphi = 0.45$		
	$V_{hot\ water}$	$V_{solvent}$	f_w^*	$V_{hot\ water}$	$V_{solvent}$	f_w^*	$V_{hot\ water}$	$V_{solvent}$	f_w^*
Clean Sands	0.1814	0.1168	0.9607	0.4271	0.1168	0.9076	0.7132	0.1168	0.8496
Clayey Lime	0.1661	0.1168	09641	0.3982	0.1168	0.9137	0.6797	0.1168	0.8561

Table 1.2. The influence of rock properties upon the efficiency of miscible hot WAG. It shows that the formation properties such as porosity and heat capacity of rock have major impacts over the behavior of hot water injected. The larger the formation heat capacity (and the smaller the porosity), the slower the hot water front travels (the more hot water needs to be injected).

1.5. Conclusions

1) Miscible hot WAG manifests itself as an efficient EOR method for recovery of (slightly) heavy oil compared to cold WAG and hot water flood. Its main advantage lies in the improvement of sweep efficiency, when the hot water bank ahead of the gas bank significantly reduces the mobility ratio at the solvent-oil displacement front.

2) We derive a condition for an optimal WAG ratio (Eq.[1.14]) in such a process based on formation and fluid transport properties. The "optimal" process is one where the thermal front propagates just ahead of the solvent front. Then the advantages of reduced mobility ratio accrue at the solvent front without injecting unnecessary hot water. If the thermal front lags behind the miscible front, at least in 1D, then injection of hot water does not affect oil displacement.

3) The volume of hot water to be injected at the optimal WAG ratio is large (e.g, $f_w = 0.9$, nine volumes of hot water for each volume of solvent injected) for an example worked here. The process is then best sorted to a project where the rate of solvent injection is limited – e.g., using solvent from an industrial project with limited output. Then injecting large volumes of hot water need not slow down the injection of solvent.

4) Miscible hot WAG may not be an as promising EOR method for lighter oil recovery as for heavy oil: the improvement of mobility ratio is less than that for heavy oil. Formation properties (porosity, formation heat capacity, and relative permeabilities) also affect the optimal WAG ratio and dimensionless velocity of the displacement front.

5) To fully explore this issue, fine-grid 2D and 3D reservoir simulations, accounting for heterogeneity, channeling and gravity effects are needed.

6) In our model, we do not consider the possible effect of temperature on miscibility of the solvent.

Chapter 2-Simulation Study of Gravity-Segregation in non-Horizontal Reservoirs

WAG (Water-Alternating-Gas injection) is a non-thermal EOR technique proposed to improve the volumetric sweep efficiency and consequently the oil recovery during a gas-injection project. Though miscible gas injection renders excellent displacement efficiency due to its miscibility with oil, it usually shows very poor volumetric sweep efficiency due to its high mobility. The mobility of gas is lowered by an alternate injection of gas and water, and the gas fingering effect is thus mitigated. Aside from the effect of gas fingering, gravity-segregation is another destructive factor to volumetric sweep efficiency. The gas and water injected, due to density difference, begin to segregate apart from each other under gravitational forces. Gas segregates to the top of the reservoir, forming an override zone, and water goes to the bottom of the reservoir, forming an underride zone. No mobile water phase is present in the override zone; all the gas segregated from the mixed zone flows through this region without sweeping the residual oil trapped in the under-ride zone of mobile water. It is therefore crucially important to know when and where the complete segregation between gas and water happens in the reservoir, and the producing well ought to be placed in a distance within the extent of complete segregation. Stone & Jenkins created an analytical model to describe the gravity-segregation effect in horizontal reservoirs in the 1980's. This model predicts the segregation distance. It also provides good description about the geometrical character of the segregated zones, as well as prediction over the related oil recovery. Namani *et al* (2012) extended this model to applications in non-horizontal reservoirs. The main focus of this paper is, on the one hand, studying the gravity-segregation effect in non-horizontal reservoirs by numerical simulation, and, on the other hand, examining the accuracy of Namani's solution by matching the computed results from his model to the simulation outcomes.

2.1. Analytical model of gravity-segregation in non-horizontal reservoirs

Stone's model was developed to predict the distance of complete gravity-segregation in a WAG process in a horizontal reservoir (Stone, 1982). Figure 2.1-(a) depicts Stone's image of a WAG process, approximated as a process where gas and water are co-injected along the entire reservoir interval to displace oil. Close to the injector, there is a uniform advance of gas and water; all the oil in this region comes into contact with gas. Further into the reservoir, gas and water begin to segregate under gravitational force. Gas goes to the reservoir top forming a thin gas streak, while water goes to the bottom of the reservoir. After steady state is reached, the reservoir can be divided into three distinct zones: (1) a uniform mixed zone, where gas is flowing at intermediate water saturation, which results in lower gas relative mobility; (2) an override zone, where gas is the only mobile phase, and its relative mobility is significantly higher than the gas flowing in the mixed zone; (3) an underride zone, where water is the only mobile phase, and no gas is present. Stone's model also assumes incompressible phases, negligible capillary pressure, and the absence of inter-phase mass transfer. Jenkins implemented Stone's model, based on the same assumptions, to predict the geometry of each zone at steady state, as well as the related oil recovery (Jenkins, 1984).

Stone & Jenkins' model for a horizontal reservoir has been broadly examined with numerical simulations. In the meantime, rigorous proof for the model was done with application of the stream function as well as the fractional-flow theory (Rossen, van Duijn, 2010)**.** Yet we still know little about the process of gravity segregation in non-horizontal reservoirs; Rossen & van Duijn's derivation of Stone's equation can't be extended to dipping reservoirs. Namani *et al.*(2012) developed an analytical model to predict these segregation distance in dipping reservoirs (Eq. [2.4]). The segregation distance $L_{g,dip}$ in his model is the distance along the dipping direction of the reservoir. Namani's model, while making all the assumptions made by Stone & Jenkins, attempts to embrace the effects of reservoir dip (Figure 2.1-(b)). For horizontal reservoirs, fluid flow can be divided into two components: the flow along the reservoir driven by horizontal pressure gradient, and the vertical segregation of fluids produced by gravitational force. The gravitational potential gradient is perpendicular to the overall flow direction in the reservoir. For non-horizontal reservoirs, however, the gravitational potential is partly aligned with the flow along the reservoir and is different for the two phases.

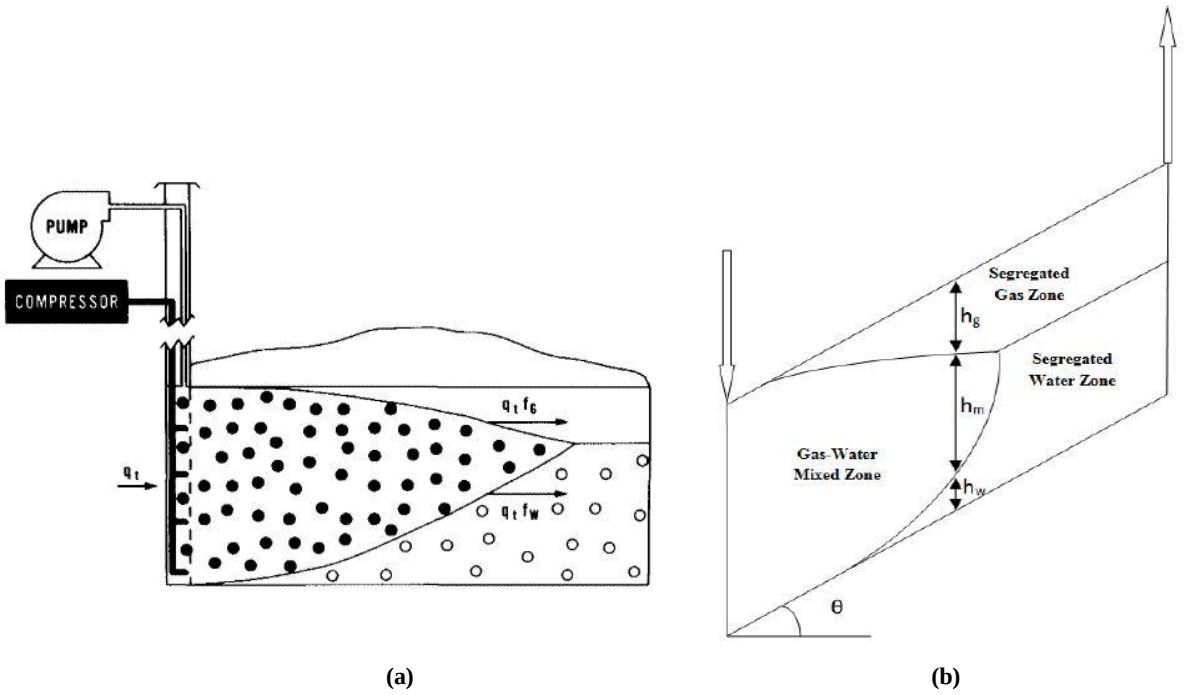

(a) **(b)**

Figure 2.1. Schematic illustration of gravity segregation. (a) Gravity segregation in horizontal reservoir (Stone, 1982). (b) Gravity segregation in down-dip injection (Namani, 2012).

Unfortunately, a key assumption of Namani's model is incorrect. For Darcy flow in horizontal reservoirs, the horizontal pressure gradient of both gas and water phase are equal. Therefore, both WAG ratio and fractional flow rate f_w are dependent on only the ratio of phase relative mobilities. For dipping reservoirs however, there exists a hydraulic build-up between injector and producer, and Darcy flow on both direction (along and perpendicular to the reservoir dip) therefore depends on the gradient of phase potentials instead of pressures. Namani *et al.*(2012) claim that, though the phase pressure gradients for gas and water (equal in horizontal reservoirs) are different in dipping reservoirs, the potential gradient of each phase should equal to each other. Therefore, the fractional flows and WAG ratio, as in Stone's derivation, are again dependent on the ratio of phase relative mobilities only (Namani, 2012, Equation (1)-(15)). This assumption is incorrect in general (Eq.[2.1]-[2.3]). WAG ratio is determined by water volumetric injection rate q_w and gas volumetric injection rate q_g(Eq.[2.1]). H_g and H_w are the thickness of override zone and under-ride zone, and λ_{gg} and λ_{ww} are the gas relative mobility in override zone and water relative mobility in under-ride zone (Eq.[2.2]).$\Phi_{g,x}$ and $\Phi_{w,x}$ are the gas and water flow potential along the reservoir direction (Eq.[2.3]).

$$\mathrm{WAG} = \frac{q_{w,x}}{q_{g,x}} = \frac{K_h \left(\frac{k_{rw}}{\mu_w}\right)_m \left[\frac{dP_w}{dx} + \rho_w g \sin(\vartheta)\right]}{K_h \left(\frac{k_{rg}}{\mu_g}\right)_m \left[\frac{dP_g}{dx} + \rho_g g \sin(\vartheta)\right]} = \left(\frac{k_{rw}}{k_{rg}} \cdot \frac{\mu_g}{\mu_w}\right)_m \cdot \frac{\nabla\Phi_{w,x}}{\nabla\Phi_{g,x}} \qquad \textbf{Eq.[2.1]}$$

$$\frac{H_w}{H_g} = \mathrm{WAG} \cdot \frac{\lambda_{gg}}{\lambda_{ww}} = \left(\frac{\lambda_w}{\lambda_g}\right)_m \cdot \left(\frac{\lambda_{gg}}{\lambda_{ww}}\right) \cdot \frac{\nabla\Phi_{w,x}}{\nabla\Phi_{g,x}} \qquad \textbf{Eq.[2.2]}$$

$$f_w = \frac{q_{w,x}}{q_{w,x} + q_{g,x}} = \frac{1}{1 + \left(\frac{k_{rg}}{k_{rw}} \cdot \frac{\mu_w}{\mu_g}\right)_m \cdot \frac{\nabla\Phi_{g,x}}{\nabla\Phi_{w,x}}}$$ **Eq.[2.3]**

Namani's model states that the segregation distance for a dipping reservoir $L_{g,dip}$ is that for a horizontal reservoir $L_{g(Stone)}$ divided by $\cos(\vartheta)$ (Eq.[2.4]).

$$L_{g,dip} = \left[\frac{q_t}{\Delta\rho g \cdot K_v \cdot W \cdot \left(\frac{k_{rw}}{\mu_w} + \frac{k_{rg}}{\mu_g}\right)_m}\right] \times \frac{1}{\cos(\theta)} = \frac{L_{g\,(Stone)}}{\cos(\theta)}$$ **Eq.[2.4]**

The cosine function is symmetrical **about** zero ($\cos(\vartheta) = \cos(-\vartheta)$ for $\theta \in \left[-\frac{\pi}{2}, \frac{\pi}{2}\right]$). As a result, Namani claims that the segregation distance is the same for both up- and down-dip injection, and the advantages of them are nearly equal. Additionally, he claims that in the up-dip case the hydraulic head can help to obtain a greater flow potential compared to down-dip injection, and this increased flow potential results in an additional total flow rate that can slightly extend the mixed zone (Namani *et al*, 2012)

Although the assumption of identical potentials is not rigorously true, Eq. [2.4] might still be a useful approximation. We examine this with numerical simulation.

2.2. Numerical simulation for non-horizontal reservoirs

2.2.1. Model description

A series of numerical models have been implemented in Eclipse100 (Schlumberger) to analyze gravity-segregation in homogeneous dipping 2-D reservoirs. Anisotropy is not forbidden by Stone's assumptions. However, in order to eliminate any possible uncertainty about the meaning of horizontal and vertical permeability in a dipping reservoi, isotropic permeabilities are assumed, as in Namani *et al*. (2012). The reservoir aspect ratio of the base case model is 160: 25 (Figure 2.2). At steeper dipping angles (especially for down-dip injection), a dimension of 120: 25 is applied in order to reduce the strong impact of hydraulic head. The reservoir and fluid properties are partly taken from Namani (2012) and given in Table A.4. A black-oil model is used in our analysis. It was initially suspected that the solution-gas capacity of oil "R_s" may have an effect over the segregation distance. Setting the solution gas ratio to a constant may eliminate any complications involved. However, simulation later show that the presence of solution gas exchange doesn't influence the reservoir condition at steady-state. We therefore implement the model with more realistic PVT properties (Table A.4). Namani's study also showed that the alternative between a compositional model and a black-oil model doesn't make significant difference in the final results, which gives another convincing reason to use a black-oil model.

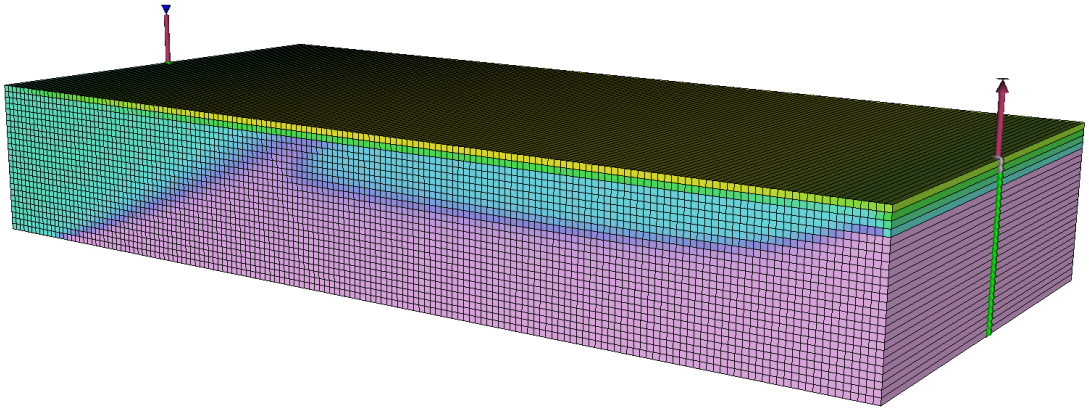

Figure 2.2. 3-Dimensional view of base-case model. Injector and producer are perforated over the entire reservoir interval.

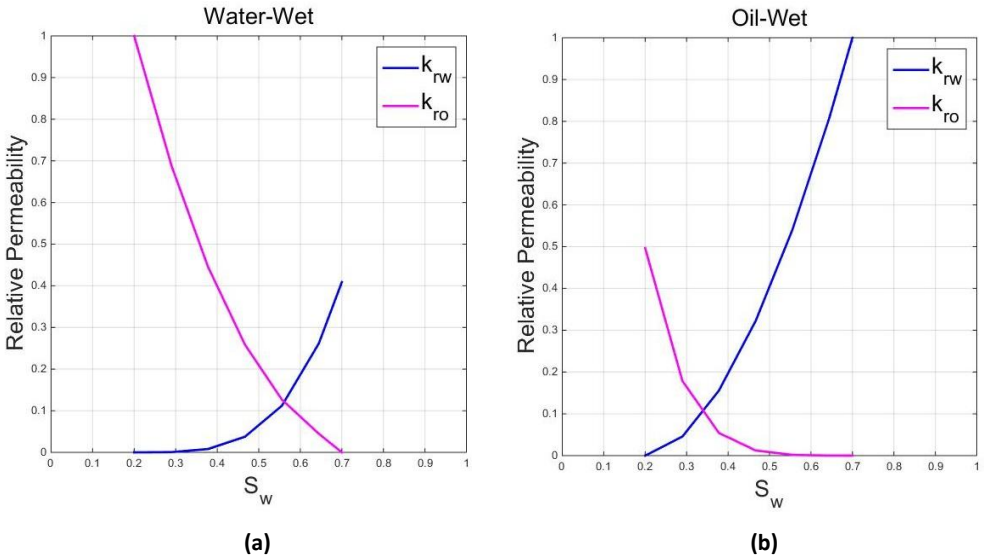

Figure 2.3. Phase relative permeability. (a) Water-wet system. (b) Oil-wet system.

Stone & Jenkins' model assumes that the reservoir is initially saturated with oil, and a solvent that's miscible with oil is injected. A "Miscible Flood Model" (a built-in function in Eclipse 100) was therefore invoked in the numerical model to represent a miscible flood. This model describes the miscible flooding process of a three-component system. The Todd-Longstaff parameter is used in the black-oil model to account for the alteration of phase properties due to mixing. There are two parameters $(\omega, \alpha) \in [0,1]$. The first term ω determines the effective gas and oil viscosities in the mixture. The second term α defines the degree of miscibility by weighing between the relative permeability of immiscible flood and the relative permeability of fully miscible flood. $\alpha = 0$ suggests a fully immiscible flood, while $\alpha = 1$ suggests a fully miscible process (Jåkupsstovu *et al*, 2001). In our simulations, a value of 1.0 is applied.

Like Stone & Jenkins, we assume simultaneous injection of gas and water as an approximation of alternate slug injection. This is justified as long as the injection cycles are very short (Stone, 1982).

2.2.2. Base-case analysis

Three base-case simulations are done to analyze the fundamental characteristics of gravity-segregation in non-horizontal reservoirs. A case of a horizontal reservoir and two cases of non-horizontal reservoirs (20° dip up-dip injection and down-dip injection). In base case a water-wet system is assumed (Figure 2.3-(a)), a total injection rate of 9000 reservoir bbl (RB)/day with a WAG ratio of 1:1 is used. Refer to table A.4 for other reservoir and fluid properties.

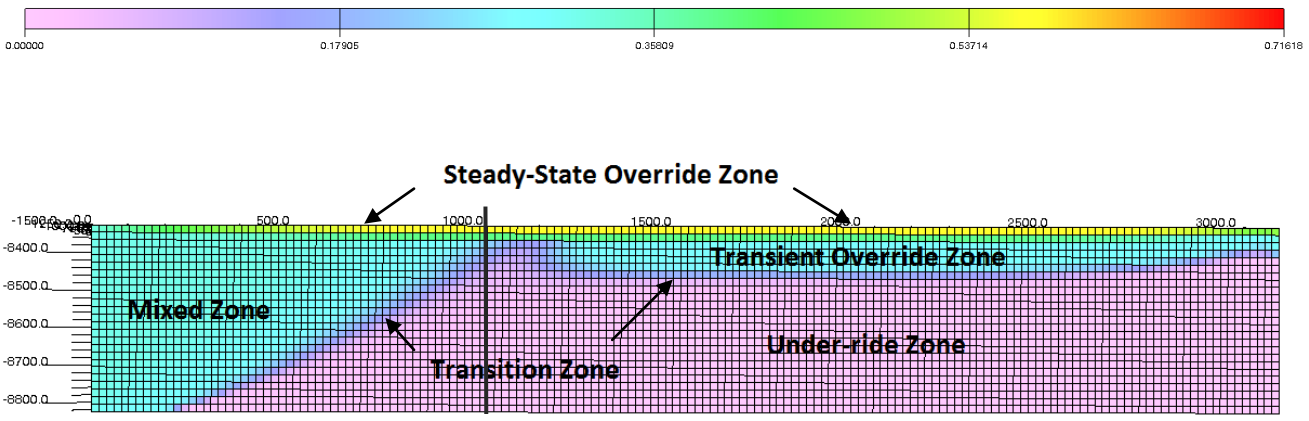

Figure 2.4. Base-case-1. Gas saturation distribution at steady-state in a horizontal reservoir. Total injection rate $q_t = 9000$ RB/day, WAG=1.$\omega = 0$.

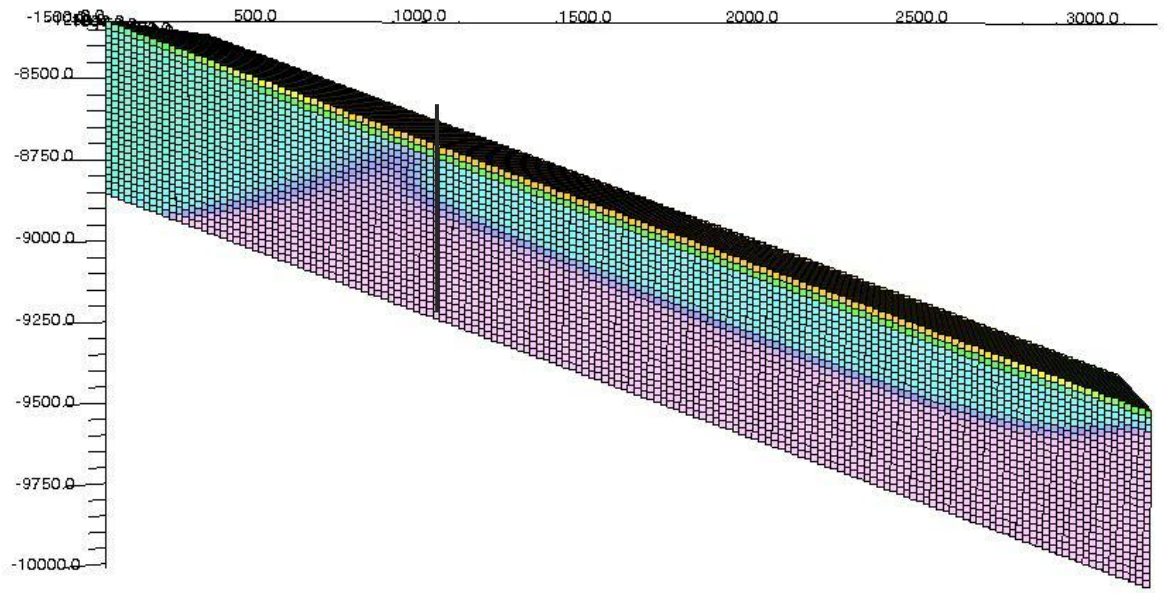

Figure 2.5. Base-case-2. Gas saturation distribution at steady-state in a 20° dip reservoir with up-dip injection. Total injection rate $q_t = 9000$ RB/day, WAG=1.

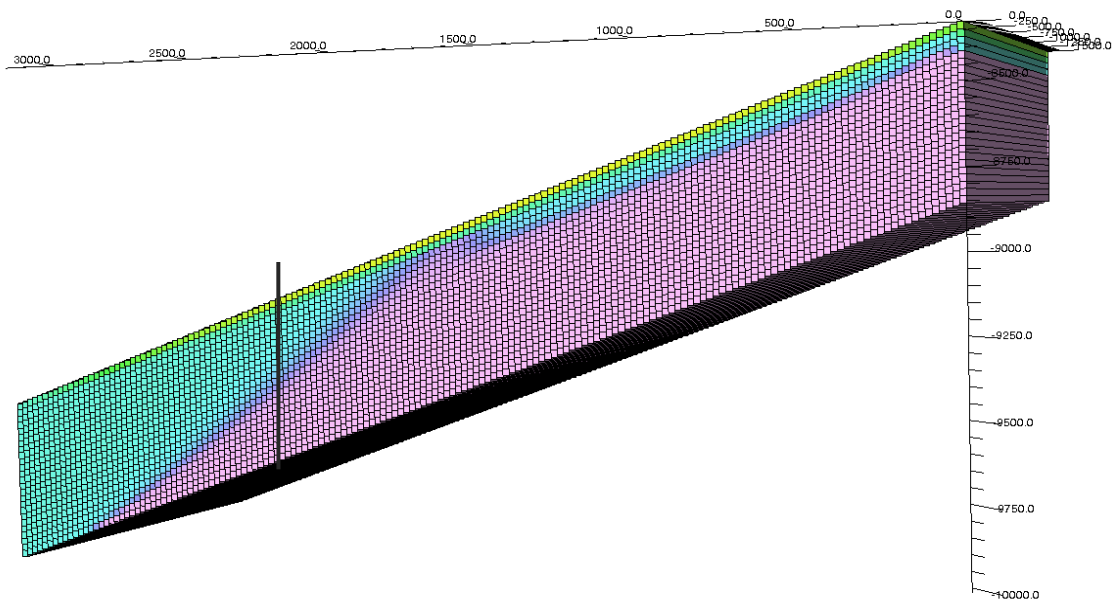

Figure 2.6. Base-case-3. Gas saturation distribution at steady-state in a 20° dipping reservoir with down-dip injection. Total injection rate $q_t = 9000$ RB/day, WAG=1.

Figure 2.4-2.6 illustrates gas saturation at steady state. From previous studies, most of the main features of gravity-segregation can be predicted and described by existing models. The model of Stone & Jenkins provides a good description of the segregation distance, the geometry of the mixed zone, the override and under-ride zones.

2.2.2.1. Geometry of segregated zones

Beyond the end of the mixed zone, the reservoir at steady-state can be divided into three sections: the underride zone, the transient override zone and the steady-state override zone (Figure 2.4). We address three issues here: (1) the thickness of steady-state override zone; (2) the thickness of the transient over-ride zone; (3) the complete segregation distance. The thickness of steady-state override zone can be determined from Eq. [2.2], and thickness of the transient override zone from Eq. [2.5]. The thickness of override zones increases with dipping angle in up-dip injection, and decreases with dipping angle in down-dip injection (Figure 2.5-2.6).

A black vertical line is drawn at the location computed from analytical model (Figure 2.4-2.6) for the extent of the mixed zone (Eq.[2.4]) to compare with the simulation result (Figure 2.4-2.6).As discussed above, the analytical model suggests that the horizontal distance ($L_{h,dip} \equiv L_{g,dip}/\cos(\vartheta)$) of complete segregation for all dipping angles should be identical. In the base case, the horizontal distance of segregation (Eq.[2.4]) is 1030ft (Figure 2.4). The complete segregation distances for both up-dip(Figure 2.5) and down-dip injection (Figure 2.6) are compared to the horizontal case. The segregation distance for up-dip injection doesn't extend as far as the $L_{g,dip}$ in Eq.[2.4].For down-dip injection it stretches longer than the computed result. In order to get a clearer view of gravity segregation in non-horizontal reservoirs, simulations with more dipping angles are presented below.

2.2.2.2. Transition zone and mixing parameter

One aspect that's beyond the grasp of the analytical model, however, is the occurrence of a transition zone between the regions filled with gas and the regions filled with oil (Figure 2.4-2.6). The analytical model assumes sharp boundaries between each zone. But the presence of dispersion leads to a gradual transition and the sharp boundaries

disappear. Previous study has ruled out the possibility of numerical dispersion by doing grid refinement (Namani, 2013). The size/thickness of the transition zone for a fully miscible flood is determined by the first term of the Todd-Longstaff mixing parameter $'\omega'$ (J åkupsstovu *et al*, 2001). A value of $\omega = 1$ suggests that gas and oil flow at their own viscosities without any influence from the mixing, which leads to thinner transition zone and sharper boundaries. While $\omega \in [0,1)$ suggests that the viscosity of oil and gas should be altered according to the level of mixing, and their effective viscosities are dependent upon the gas-oil mixture viscosity, leading to a gradual transition between gas and oil viscosities and hence a thicker transition zone (Figure 2.7).

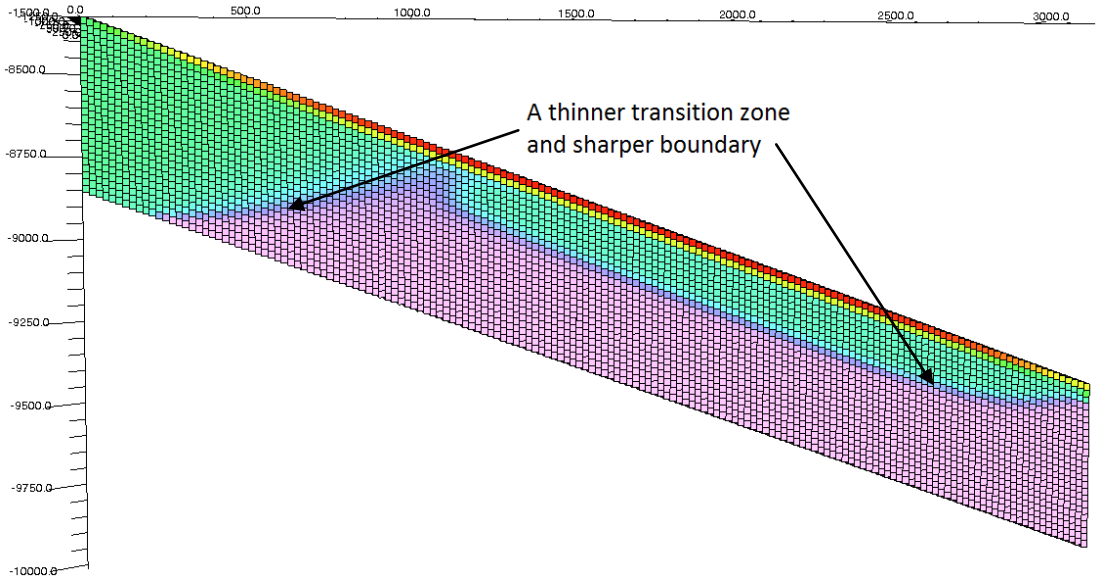

(a)

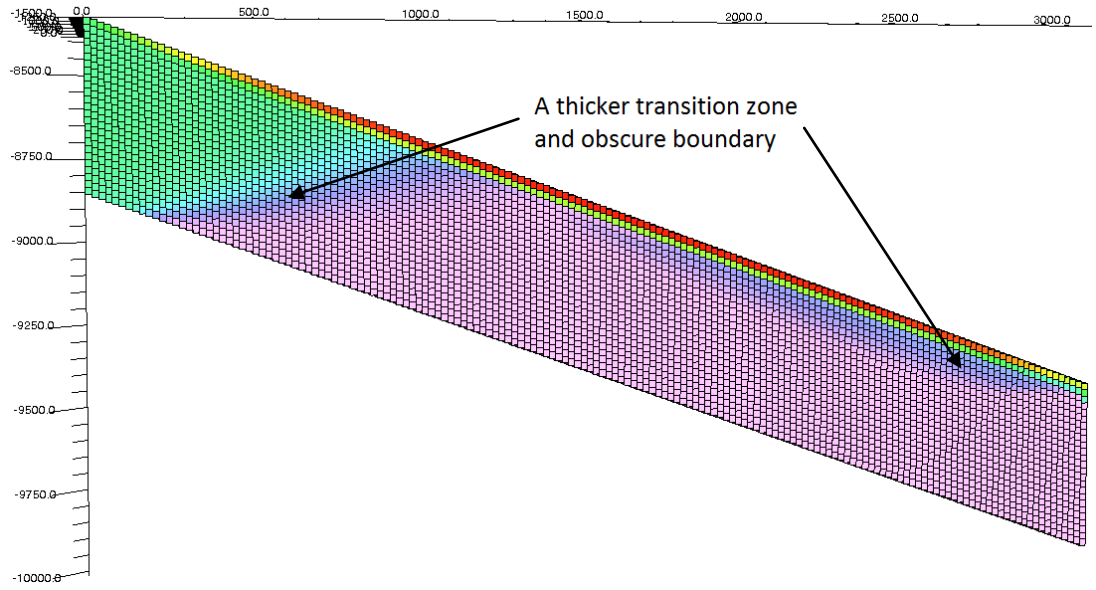

(b)

Figure 2.7. Todd-Longstaff mixing parameter and the thickness of transition zone. (a)20°up-dip injection. ω=1.0, $\alpha = 1.0$. $q_t = 9000$ RB/day, WAG=1. Gas and oil viscosities are not influential to each other. A sharp (relatively) boundary exists between mixed zone and under-ride zone. (b)20°up-dip injection. ω=0.0, $\alpha = 1.0$. $q_t = 9000$ RB/day, WAG=1. The effective viscosities of gas and oil strongly dependent on their mixture viscosity. There is a gradual transition from gas to oil, sharp boundary disappears.

2.2.2.3. Transient Override Zone

Another important effect that's not included in the analytical models is the occurrence of a gas advance (Figure 2.4) in the water-segregated zone due to what Namani calls the Transient Time Effect. In the following, we refer to this zone of gas advance as the "Transient Override Zone". Stone's model claims that the reservoir, at steady-state, can be divided into three separated zones, and based on which assumption Jenkins' model was developed to describe the geometry of each zone as well as to predict the corresponding oil recovery. Unfortunately, none of these models provides prediction and explanation of this transient effect, which breaks Stone's assumption of the reservoir being divided into three uniform regions. It arises before Stone's assumption of steady state is valid.

As the injected gas pushes further into the reservoir, it tends to segregate vertically to the top and accumulate. This accumulation of gas steaks through towards the producing well and forms an override zone at the reservoir top (Figure 2.8-(a)). According to Eq.[2.3]& Eq. [2.5], the thickness of overriding zone is inversely proportional to the relative mobility of the gas in it. The transient override zone is formed because gas relative mobility is lower as gas first displaces oil and water than at steady-state condition. The gas accumulated at the top flows with lower mobility due to its lower saturation and the effects of gas-oil mixing. Lower gas mobility therefore leads to a thicker override zone early on then at steady state, when gas saturation is higher in the override zone (Figure 2.8-(a)). The thickness of over-/under-ride zone at transient stage can be determined by Eq. [2.5].

$$\frac{H_w}{H_g} = WAG \cdot \frac{\lambda_{g.tran}}{\lambda_{w,tran}} = \left(\frac{\lambda_w}{\lambda_g}\right)_m \cdot \left(\frac{\lambda_{g.tran}}{\lambda_{w.tran}}\right) \cdot \frac{\nabla\Phi_{w,x}}{\nabla\Phi_{g,x}} \qquad \textbf{Eq.[2.5]}$$

Eq. [2.5] is in nature the same as Eq. [2.3], only that $\lambda_{g,tran}$ and $\lambda_{w,tran}$ are now the transient-state phase mobilities in the override gas zone. As steady-state is approached, mobile water segregates to the under ride zone and only connate water remains on top. In addition, all the oil initially present is displaced. This leads to a condition when gas is the only mobile phase in the override zone (Figure 2.8-(b)). Higher gas saturation and the absence of oil result in higher gas relative mobility. At steady-state, the gas in the override zone escapes to the top, which ultimately results in a thinner override zone (Figure 2.8-(c)). Therefore, the "transient override zone" could also be called "the developing (dynamic) override zone", when reservoir and fluid properties are constantly changing, and the thickness of over-/under-ride zones continuously adjusts according to the relative mobilities. The "steady-state override zone" could also be called "the developed (static) override zone", when everything in the reservoir is settled down and remains constant.

The model of Stone & Jenkins is a static model designed to depict steady state. However, the transient reservoir condition before steady-state does affects its steady-state condition. As we mentioned above, a portion of the gas in transient zone eventually leaves, resulting in a thinner override zone. But, gas could be trapped in there permanently by capillary forces (Figure 2.8-(c)). The amount of gas trapped depends on the transient flow. Phase relative permeability, phase viscosity, initial oil saturation S_{oi} and Todd-Longstaff mixing parameter all have an effect on the transient gas mobility. They together determine the amount of trapped gas. The gas left in the transient zone leads to lower S_w at the top of the underride zone, and therefore lower average relative mobility of water phase λ_{ww} (Eq. [2.3]). Consequently, the steady-state override zone should be a little thinner than what's predicted by the analytical model (when the trapped gas is present). The more gas is trapped (the thicker the transient override zone), the thinner the steady-state over-ride zone would be.

The analytical model assumes that the reservoir, when at steady-state, can be divided into three zones. It assumes that the mixed zone and override zone are swept by gas with no residual oil left, while under-ride zone is swept by water and leaves residual oil behind (Figure 2.1). With the presence of the transient override zone, however, part of oil in the under-ride zone can also be completely displaced by miscible gas, which leads to extra oil production (Figure 2.9). In some cases, most of the oil recovery is contributed by the transient override zone, and the effect of mixed zone becomes less relevant.

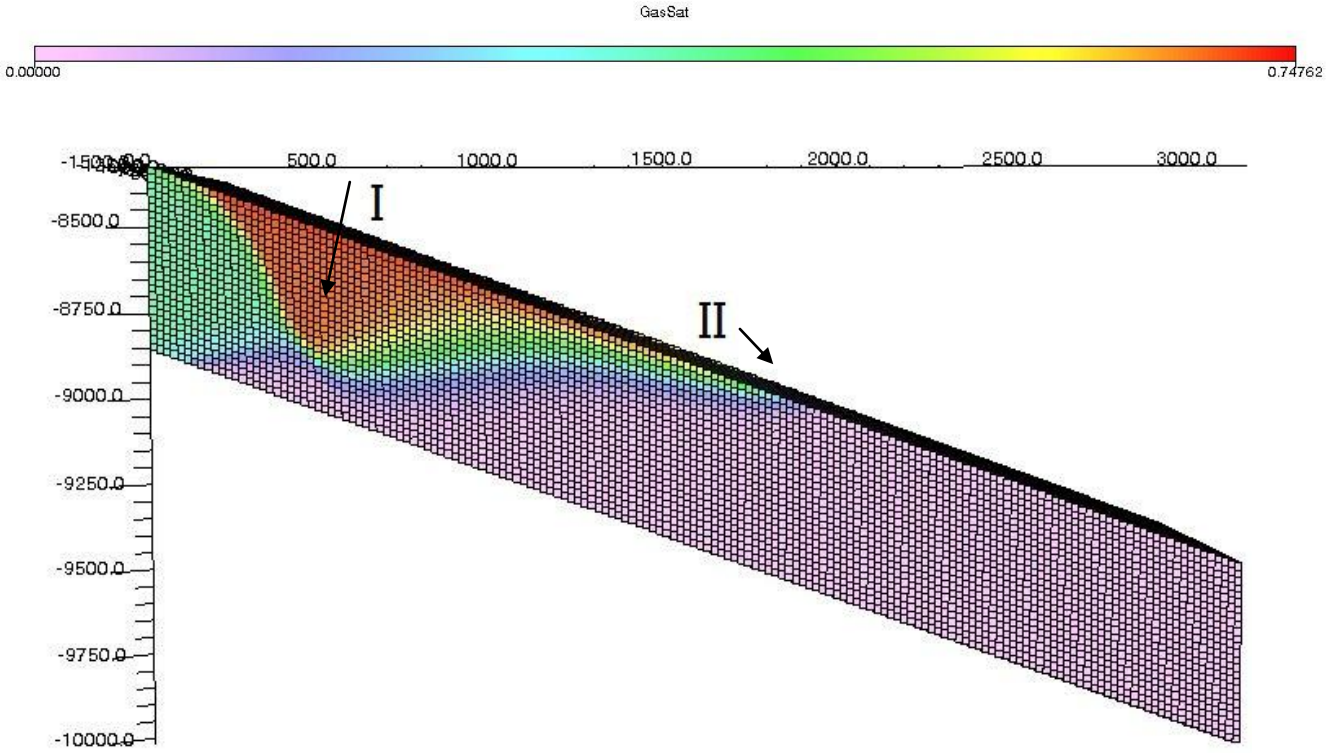
GasSat
0.00000
0.74762
500.0
1000.0
1500.0
2000.0
2500.0
3000.0
-8500.0
-8750.0
-9000.0
-9250.0
-9500.0
-9750.0
-10000.0
I
II

(a)

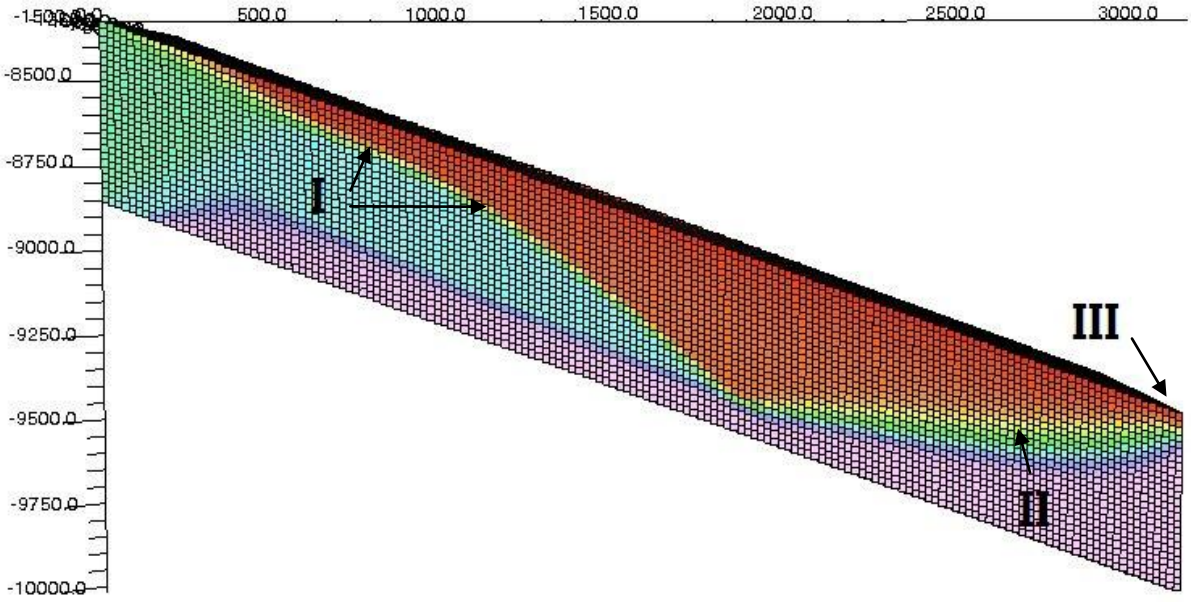
500.0
1000.0
1500.0
2000.0
2500.0
3000.0
-8500.0
-8750.0
-9000.0
-9250.0
-9500.0
-9750.0
-10000.0
I
III
II

(b)

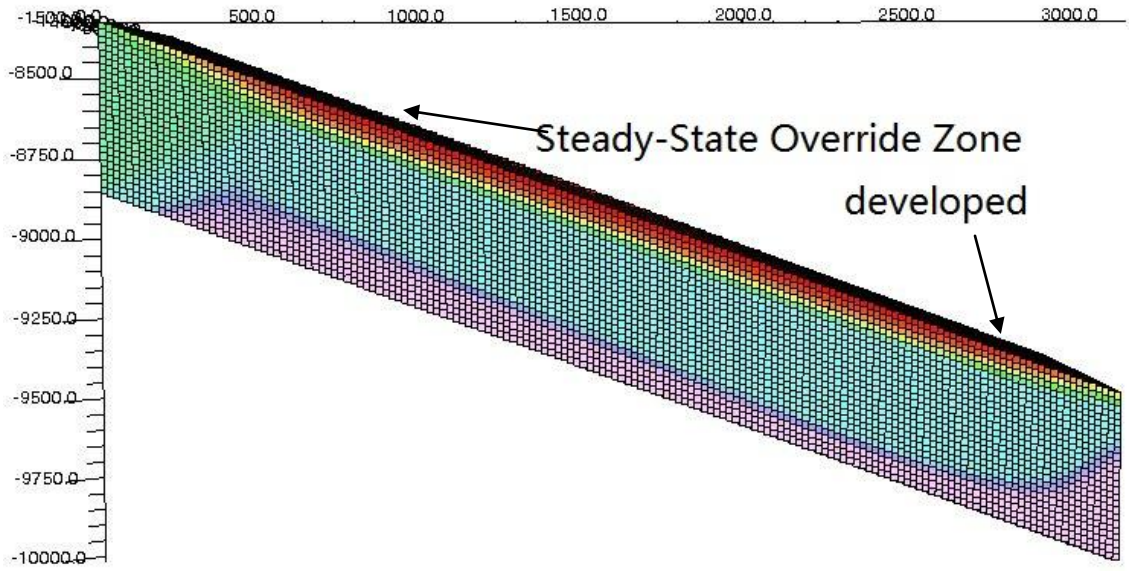

(c)

Figure 2.8. The development of transient override zone. $q_t = 12500$ RB/day, WAG=1:4 (0.25). (a) The beginning of transient override zone at early stage of injection, when the gas relative mobility is lower than that of the steady-state due to lower saturation. (Ⅰ)Gas bank accumulates on top. (Ⅱ)Gas trying to break through from reservoir top. (b) The formation of gas streak after the gas breakthrough results in higher gas mobility in the override zone. Water begins to invade into the lower part of transient override zone. The transient under-ride zone grows thicker and thicker, while the transient override zone grows thinner and thinner. The thickness of transient override zone is determined by Eq. [2.5]. (Ⅰ)Gas leaving transient override zone. (Ⅱ)Transient override zone is developing. (Ⅲ)Breakthrough of gas at producer. (c) The reservoir is under steady-state. The thicknesses of steady-state over-/under-ride zone can be predicted from Jenkins' model (Eq. [2.3]).

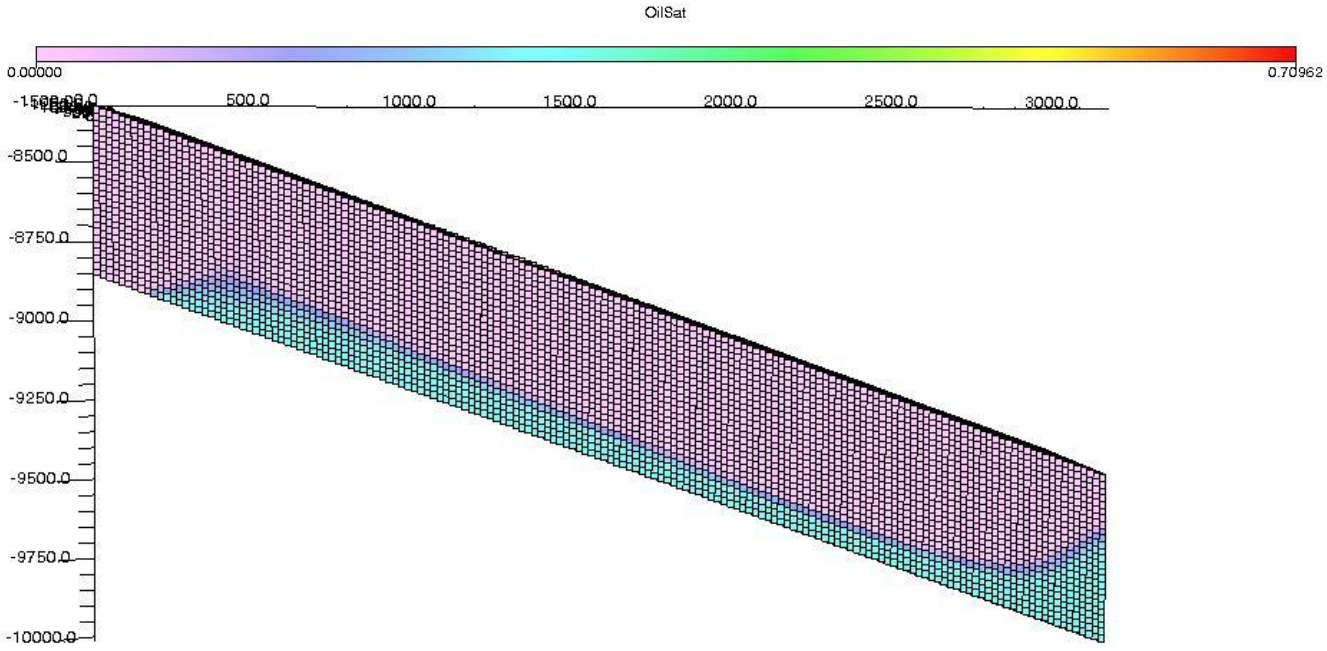

Figure 2.9. Distribution of oil saturation at steady-state for 20° up-dip injection. $q_t = 12500$ RB/day, WAG=1:4 (0.25). All the oil in the pink region has been swept by miscible gas leaving little (or no) residual oil behind.

The existing analytical model works fairly well describing the gravity-segregation effect in a horizontal reservoir. Our main focus here is testing the efficiency of Namani's extension of the model for non-horizontal reservoirs (Namani *et al*). For the horizontal the case computed result is a fairly accurate match to the simulation. Simulation results from base case show that the complete segregation distance for a 20°dipping reservoir begins to average from the prediction. The complete segregation distance for up-dip injection is a little smaller than Namani's prediction, while the result for down-dip injection appears to be a bit longer than predicted. But the deviation between simulation and computation could result from numerical errors. In particular, identifying the segregation distance from simulation results is tricky because of transition zone. Therefore, steeper dipping angles as well as various other parameters still need to be examined before we draw conclusions.

2.3. Sensitivity analysis for gravity-segregation in non-horizontal reservoirs

The analytical model by Namani *et al*. (2012) for non-horizontal reservoirs, though it lacks rigorous proof, may still be working with sufficient accuracy (at least under a specific range of conditions). In order to examine the efficiency of the model, all possible combinations of the relevant parameters ought to be tested.

2.3.1. Conformance of segregation distance in non-horizontal reservoirs

The deviation between the numerical model and the analytical model has a complex relationship with reservoir dipping angle (Figure 2.15-2.16). It is beyond the scope of this research to provide a more accurate analytical model, but we are able to explore the behavior numerically. If the segregation distance in dipping reservoirs follows a certain pattern, it will motivate the search for a mathematical model for it. Namani's model states that the horizontal projection of the segregation distance in non-horizontal reservoirs are independent of dipping angle. Numerical models, however, have shown different level of deviations from the analytical model. Let L_h represent the complete segregation distance in a horizontal reservoir (from simulation), and $L_{h,dip}$ represent the horizontal projections of segregation distance in dipping reservoirs. The segregation distance is taken here as the last grid block of the mixed zone (the end of the light blue zone in figures).Defining the dimensionless segregation distance L_D as the ratio of $L_{h,dip}$ and L_h gives:

$$L_D \equiv {L_{h,dip}}/{L_h} \qquad \textbf{Eq. [2.6]}$$

For the model of Namani *et al*, $L_D = 1$. Table C.1-C.4 (Appendix C) illustrate the effects of vertical permeability, total volumetric injection rate, WAG ratio, density difference and phase relative permeability. Though the amount of data we have is far from being exhaustive, it may suggest a pattern of $L_{g,dip}$:

$$L_{g,dip} = L_{g(\text{Stone})} \cdot F(\vartheta) \qquad \textbf{Eq. [2.7]}$$

Several conclusions can be drawn from the simulation results:

1) The dipping angle of the reservoir has a strong influence on segregation distance in up-dip injection, but has a smaller influence in down-dip injection (Figures 2.11-2.13, and 2.15-2.16).

2) The segregation distance $L_{g,dip}$ (along the dipping direction of reservoir) monotonically decreases with increasing dipping angle in up-dip injection, while it increases at shallow angles and then decreases at steeper angles in down-dip injection (Tables C.1-C.4, Appendix C. Figures 2.11-2.13, and 2.15-2.16).

3) For a particular dip angle, the dimensionless segregation distance $L_D$exhibits a decreasing trend with increasing segregation distance$L_{g,dip}$ in down-dip injection (Tables C.1-C.4, Appendix C. Figures 2.11(b)-2.13(b)). In up-dip injection it shows an increasing trend with segregation distance (Tables C.1-C.4, Appendix C. Figures 2.11(a)-2.13(a)). This tendency is very clear for vertical permeability, total injection rate, phase relative

permeabilities, but not so much for WAG ratio (Table C.2). Unlike all the other parameters, $L_{g,dip}$ has a non-linear dependency on WAG ratio. It is non-linear because the relation of WAG ratio to $\lambda_{r\alpha}$ in Eq. [2.4] is non-linear. The effect of WAG ratio on L_D is thus more complicated, and more simulations are needed before rigid conclusions can drawn.

4) The segregation distance $L_{g,dip}$ in down-dip injection, at small values, usually extends longer than that in up-dip injection (Figure 2.15-2.16). As $L_{g,dip}$ grows bigger, this effect becomes less significant due to decreasing L_D in down-dip injection and increasing L_D in up-dip injection.

5) This tendency of segregation distance needs confirmation from larger amount of simulation data. For steep reservoirs (e.g, 60°dipping reservoir), the tendency of is more observable. At shallower dipping angles, however, the tendency is relatively more ambiguous.

6) The patterns observed from simulations may suggest a non-linear relationship between $L_{g,dip}$ and its relevant parameters. Since Namani's linear function fails, and considering the difficulties of solving the problem with a pure mathematical approach, a single empirical equation doesn't' appear to apply to all data.

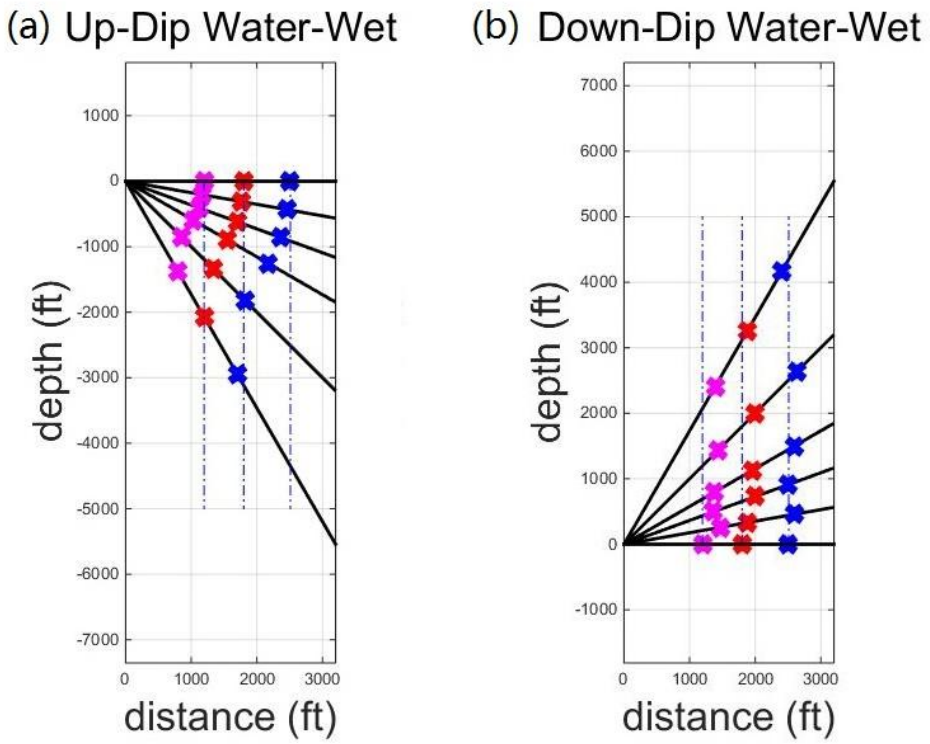

Figure 2.11. The effect of vertical permeability on segregation distance (Table C.3). (a) Segregation distances in up-dip injection. (b) Segregation distances in down-dip injection. The vertical permeabilities, from left to right (pink to blue), are $k_v = 25$md, $k_v = 15$md and $k_v = 10$md. $q_t = 10000$RB/day. WAG $= 1{:}1$ (1.0) in all three cases. L_D increases with real segregation distance in up-dip injection, and decreases in down-dip injection.

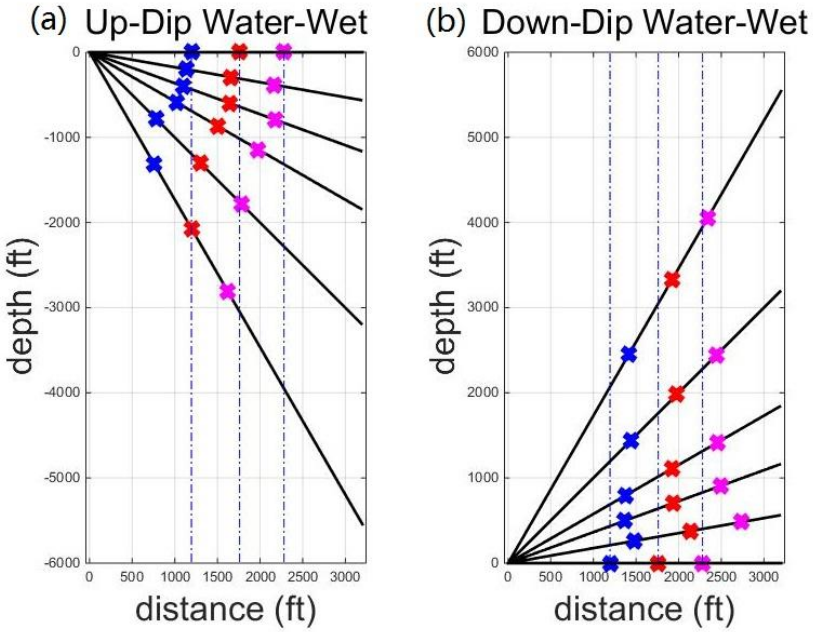

Figure 2.12. The effect of total volumetric injection rate on segregation distance (Table C.1). (a) Segregation distances in up-dip injection. (b) Segregation distances in down-dip injection. The total volumetric injection rates, from left to right (pink to blue), are $q_t = 10000$ RB/day, $q_t = 15000$ RB/day and $q_t = 20000$ RB/day. WAG $= 1:1\ (1.0)$ and $k_v = 20$ md in all three cases. L_D increases with real segregation distance in up-dip injection, and decreases in down-dip injection.

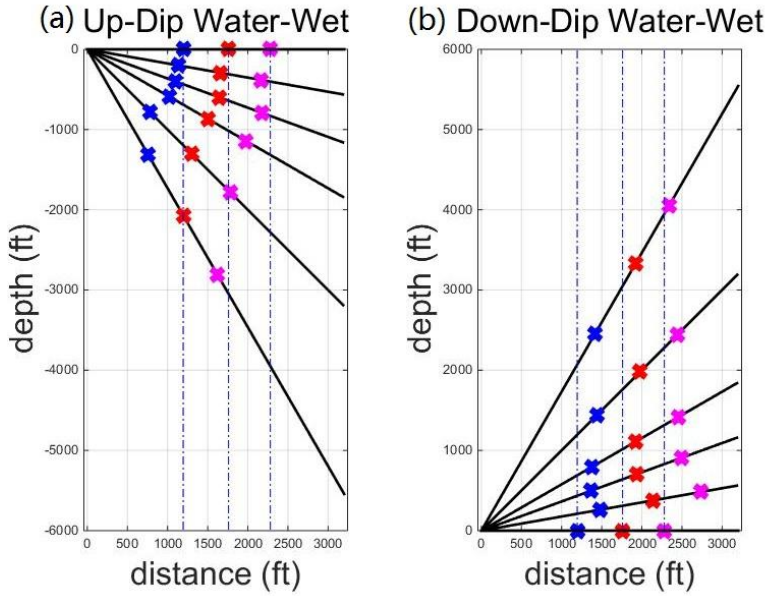

Figure 2.13. The effect of WAG ratio on distance (Table C.2). (a) Segregation distances in up-dip injection. (b) Segregation distances in down-dip injection. The WAG ratios, from left to right (pink to blue), are WAG $= 1:4\ (0.25)$, WAG $= 2:3\ (0.66)$ and WAG $= 1:1\ (1.0)$. $q_t = 12500$RB/day and $k_v = 25$md in all three cases. L_D increases with real segregation distance in up-dip injection, and decreases in down-dip injection.

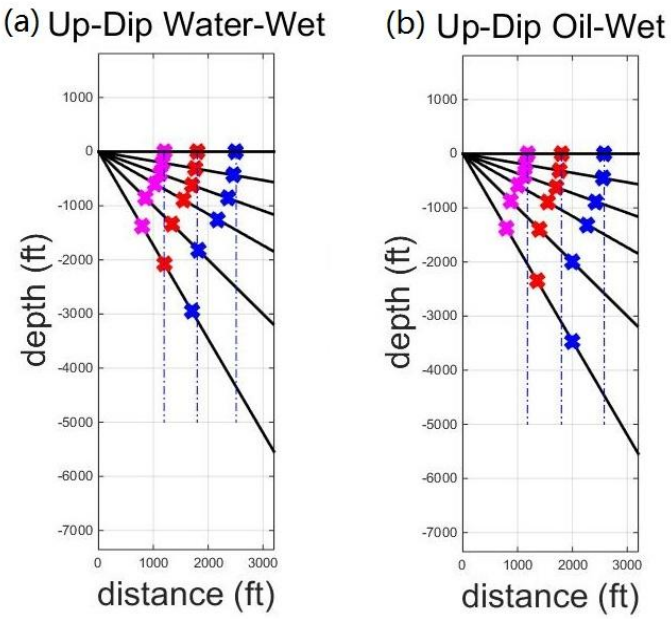

Figure 2.14. The effect of phase relative permeability on complete segregation distance (Table C.4). (a) Phase relative permeability of a water-wet system is used (Figure 2.3-(a)). (b) Phase relative permeability of an oil-wet system is used (Figure 2.3-(b)). $q_t = 10000$RB/day, WAG=1:1 (1.0) and $k_v = 25, 15, 10$md from left to right (pink to blue). In case of an oil-wet system, segregation distance stretches longer than that of a water-wet system. But $L_{g,dip}$ and L_D follows the same trend in both scenarios.

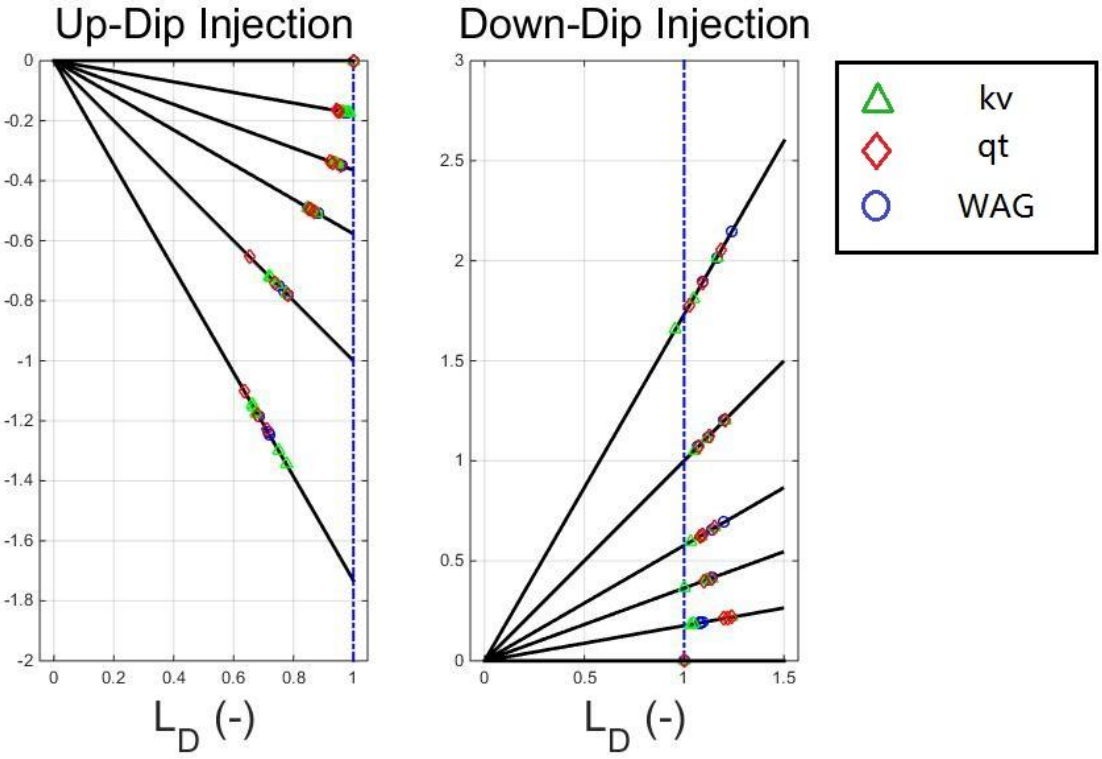

Figure 2.15. Cumulative plot of L_D for vertical permeability, total volumetric injection rate and WAG ratio.

2.3.2. Injection rate, WAG ratio

In both Stone's model and Namani's model, the complete segregation distance has a linear dependency upon the total volumetric injection rate. Figure 2.12 illustrates the effects of injection rate over segregation distance. The dependency of segregation distance on WAG ratio is included through the effect of WAG ratio on total relative mobility. However, one of their major differences is that, an increase of injection rate while keeping WAG constant requires larger injection of both gas and water; and an increase in WAG ratio while keeping total injection rate constant will demand a larger amount of water injected, but the requirement of gas injection becomes lower. Another major difference is that they have different effects on oil production through influencing the size of the gas swept zones. According to Stone's model, the well best spacing depends solely on the distance of complete segregation. Simulations have shown, however, massive production of oil is possible even after complete segregation happens. An extra amount of oil could be produced by an advance of gas sweep due to transient effect. In the examples shown, smaller WAG ratio results in a shorter segregation distance and therefore a smaller mixed zone, but it leads to a thicker override zone. And due to the effects of dipping angle we mentioned above, this scenario is particularly preferable for an up-dip reservoir, or the up-dip section of a reservoir, larger up-dip angle will result in a longer segregation distance, as well as a thicker overriding zone of gas. The disadvantage that comes along with this design, however, is the large demand for gas injection. A very large WAG ratio, on the contrary, may gain its oil production by extending the mixed zone to a longer distance, but this action could lead to a significantly thinner gas swept zone and hence a loss of oil recovery from that part of the reservoir. Therefore, there is no simple conclusion about which scenario is better for production plan. And one complication in reality is that the part of oil that's displaced by gas depends highly on the miscibility of gas, which will lead to a smaller oil recovery than what's predicted from our models.

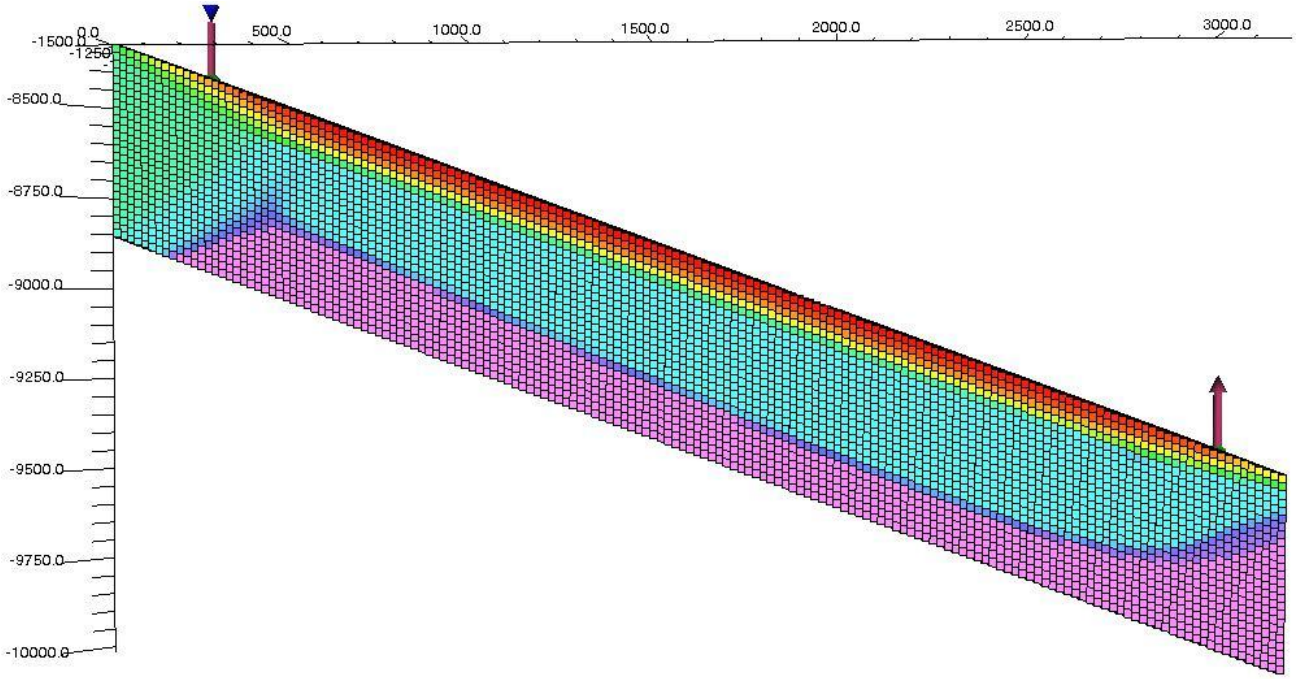

Figure 2.16. Gas saturation of a 20° dipping reservoir with up-dip injection, $q_t = 9000$RB/day, WAG $= 1:4$ (0.25).

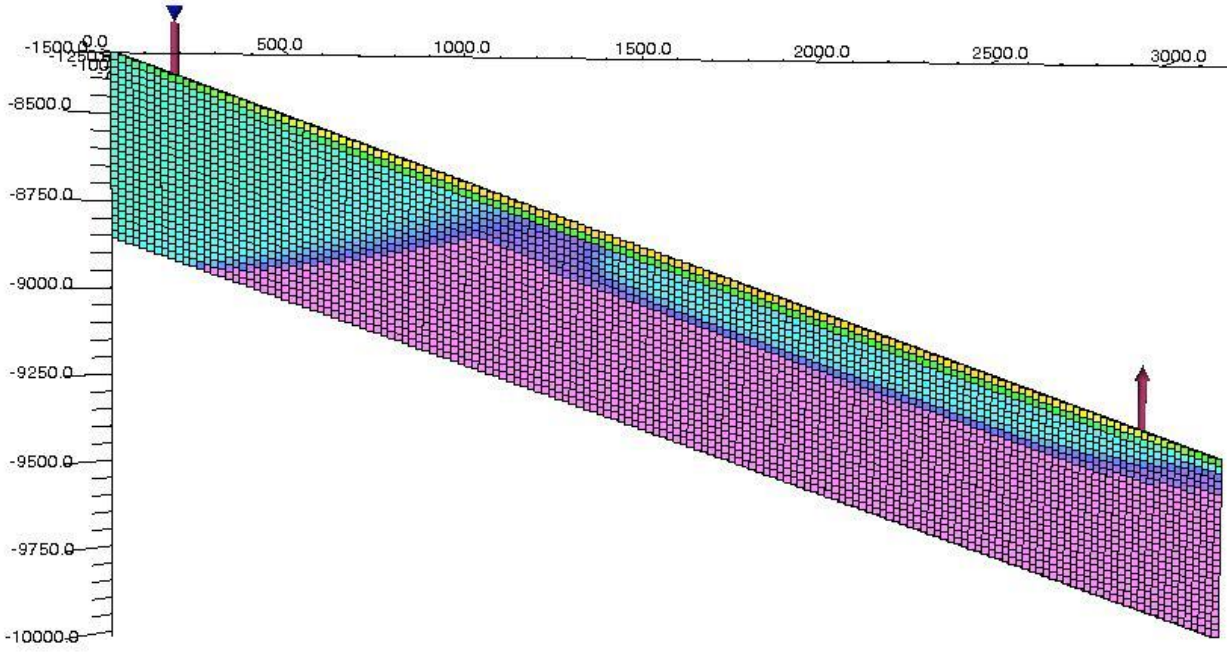

Figure 2.17. Gas saturation of a 20° dipping reservoir with up-dip injection, $q_t = 9000$RB/day, WAG $= 1:2$ (0.5).

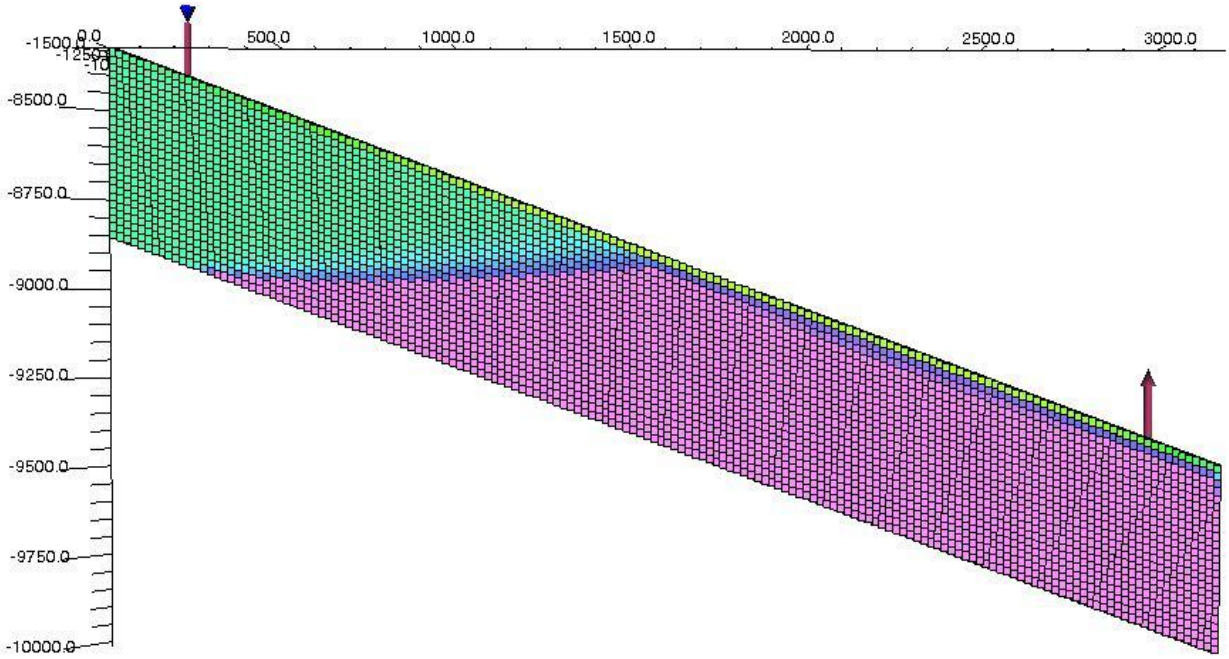

Figure 2.18. Gas saturation of a 20° dipping reservoir with up-dip injection, $q_t = 9000$RB/day, WAG $= 1:1$ (1.0).

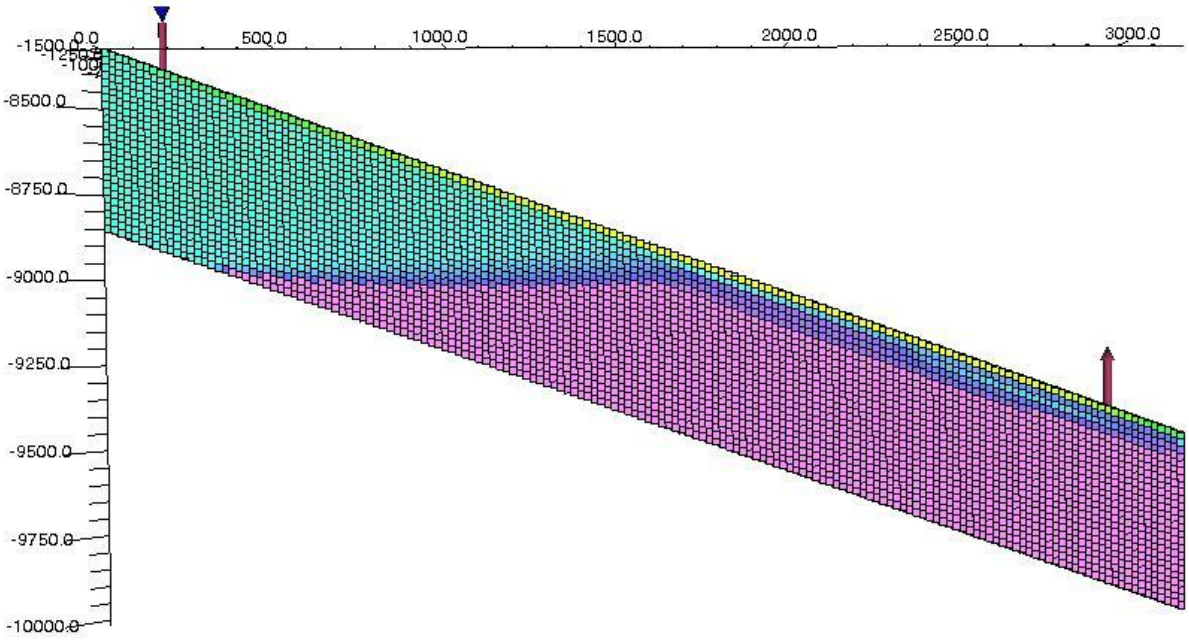

Figure 2.19. Gas saturation of a 20° dipping reservoir with up-dip injection, $q_t = 9000$RB/day, WAG $= 3:2$ (1.5).

Figure 2.16-2.19 illustrates the simulation results of a 20° dipping reservoir with up-dip injection, under various WAG ratios. These simulations aim at showing the effect of injection condition over gas sweep efficiency and hence the oil recovery. One assumption we made here is that gas supply is limited, while the supply of water is unlimited. Figure 2.16 represents a case of a small WAG ratio, in this case segregation happens very early, but gas is able to sweep most of the reservoir through the transient override zone. Figure 2.16-2.19 shows the effects of increasing WAG ratio while total injection rate is kept constant, where the segregation distance is extended with lesser amount of gas injected. But the extension of mixed zone, due to its triangular shape, doesn't seem to compensate the loss of oil production from the transient override zone of gas.

In conclusion, the optimal plan for oil production lies within the optimal combination of total injection rate, WAG ratio and well-completion design. Given the amount of resources available (gas and water), the properties of fluids, the geological condition, the costs involved in drilling & production activities, and the current oil price etc, extensive simulations and economical analysis should be done to explore the best design of injection condition.

2.3.3. The Effects of Vertical Permeability

The vertical permeability k_v is another essential factor that influences the behavior of gravity-segregation (Eq. [2.4]). Figure 2.20-2.23 illustrates the gas saturation distribution in a 20° dipping reservoir with up-dip injection, with five different vertical-permeability values. The figures show that the vertical permeability is inversely proportional to the complete segregation distance, as predicted in Eq. [2.4]. In other words, the complete segregation distance increases with decreasing k_v. However, unlike WAG ratio, the vertical permeability shows minor effects over the thickness of both steady-state and transient-state override zone. It should be justifiable to claim that the ultimate oil recovery, which is proportional to the complete segregation distance, is thus inversely proportionate to the permeability ratio. The smaller k_v there is, the larger the size of the mixed zone will be, and therefore a larger amount of oil recovery is expected.

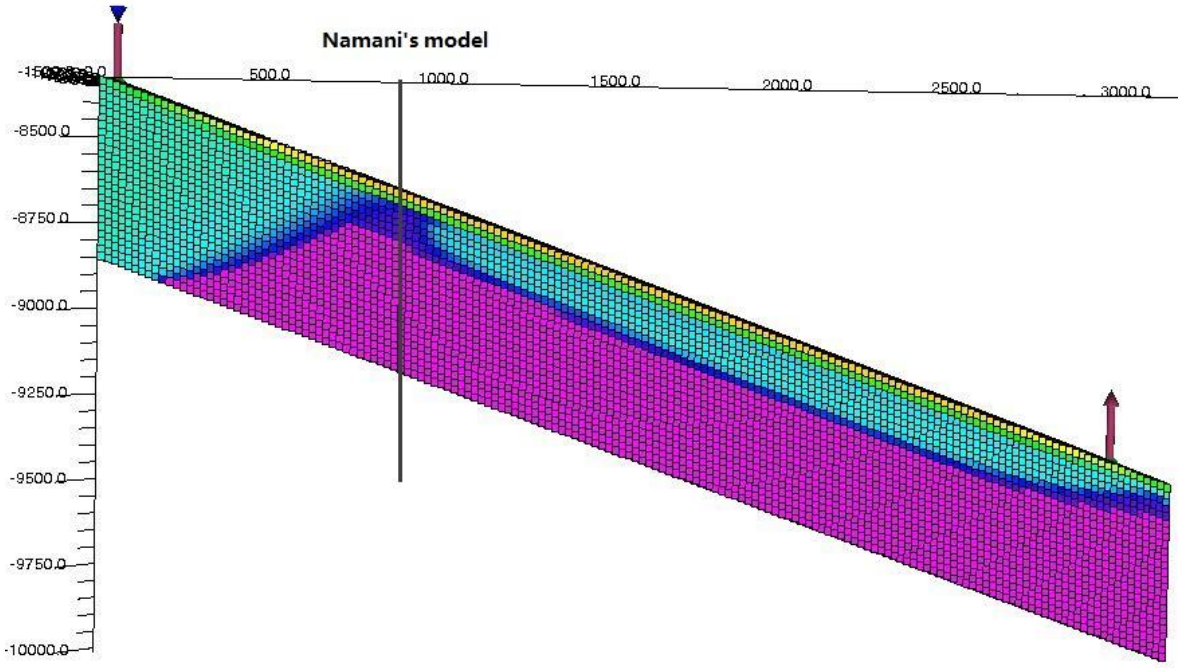

Figure 2.20. Gas saturation of a 20° dipping reservoir with up-dip injection, $q_t = 9000$RB/day, $k_v = 25$md.

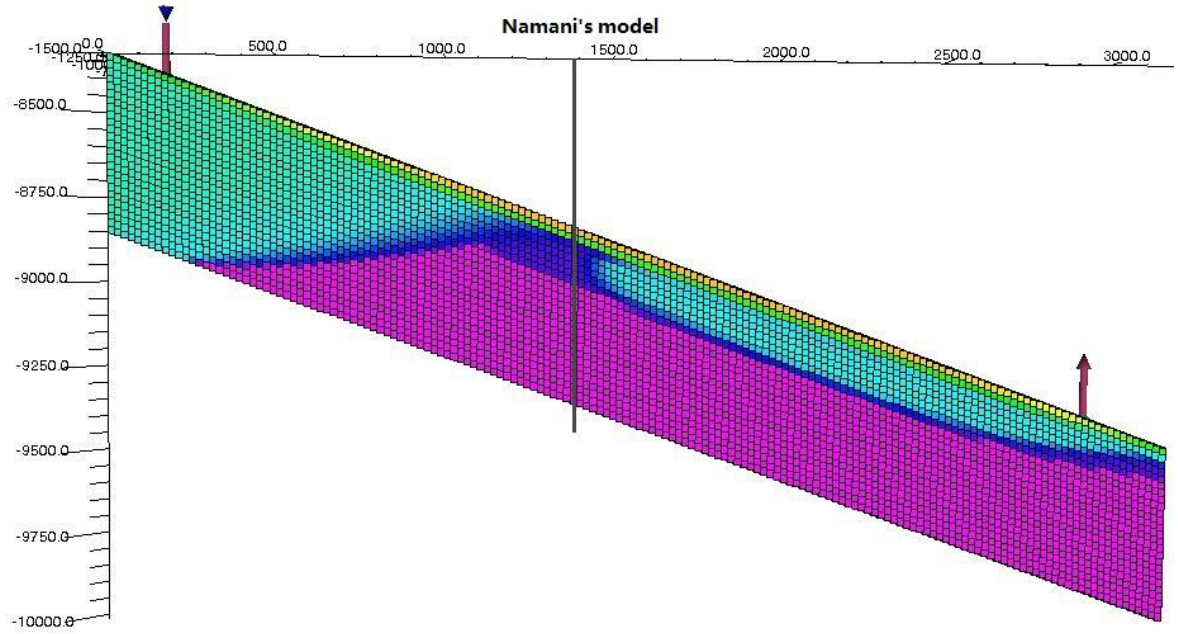

Figure 2.21. Gas saturation of a 20° dipping reservoir with up-dip injection, $q_t = 9000$RB/day, $k_v = 15$md.

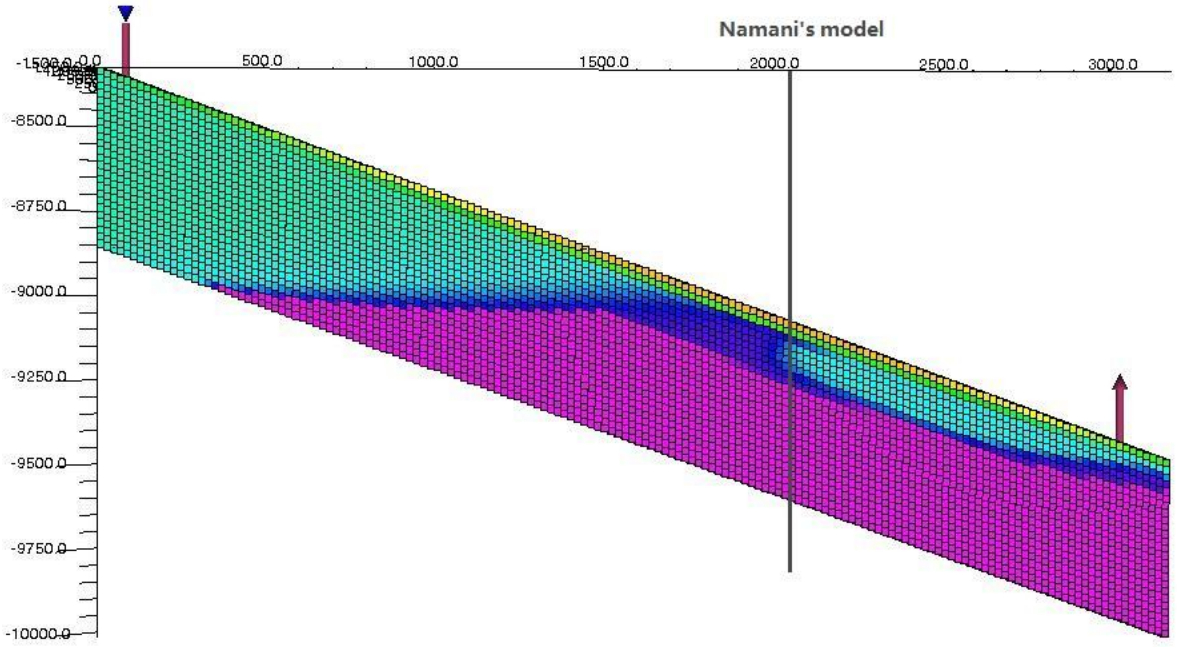

Figure 2.22. Gas saturation of a 20° dipping reservoir with up-dip injection, $q_t = 9000$RB/day, $k_v = 10$md.

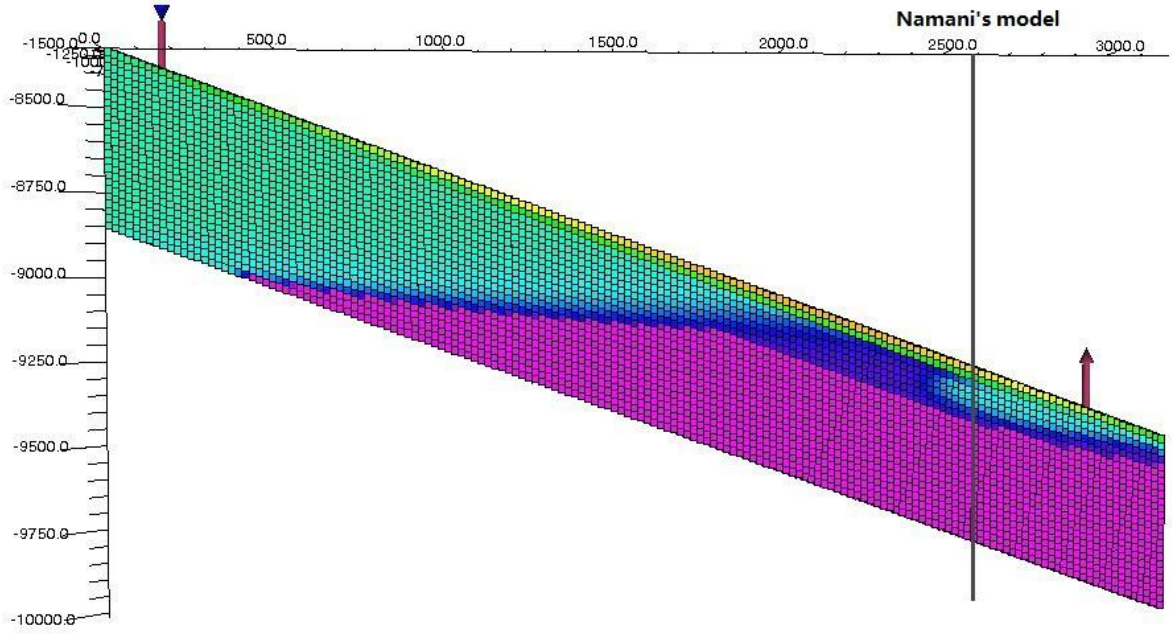

Figure 2.23. Gas saturation of a 20° dipping reservoir with up-dip injection, $q_t = 9000$RB/day, $k_v = 8$md.

2.4. Conclusions

1. Namani's assumption of identical flow potential gradient along the reservoir is incorrect. The prediction of segregation distance in dipping reservoirs, based on his model, is thus not rigorous.

2. The segregation distance in up-dip and down-dip injection follows two distinctly different trends. In up-dip injection, the deviation of segregation distance $L_{g,dip}$ from Namani's prediction grows bigger with increasing dipping angle. In down-dip injection, the deviation from Namani's model is significantly smaller than that in up-dip injection. The segregation distance increases with dip angle in shallow reservoirs, while it decreases with dip angle as the reservoir become steeper.

3. The relative segregation distance L_D, which is the ratio of L_g in dipping reservoir to that in a horizontal reservoir, increases with increasing segregation distance in up-dip injection, and decreases in down-dip injection.

4. According to simulation results, the segregation distance in a dipping reservoir follows a very complicated non-linear pattern with the relevant parameters. Rigorous mathematical proof is not available. An empirical formula may be a more practical approach.

5. The formation of transient override zone is a dynamic process that occurs during the transient stage of displacement. The occurrence of this zone, though not included in the analytical models, can be physically explained by the lower mobility of gas as it first displace water and oil from the top of the reservoir, compared to steady state.

6. The occurrence of transient override zone has a significant effect on ultimate oil recovery. By controlling the liquid fraction injected, the size of transient override zone can be adjusted. An optimal injection condition that maximizes the oil production can be achieved.

References

[1]. Buckley, S.E., and Leverett, M.C. [1941] Mechanism of Fluid Displacement in Sands. *Trans. AIME*, **146**, 107-116.

[2]. E.Ashoori, T.L.M. van der Heijden, and W.R. Rossen. [2009] Fractional-Flow Theory of Foam Displacements With Oil. *SPE 121579.* Delft University of Technology.

[3]. Herbert L. Stone. [1982] Vertical Conformance In An Alternating Water-Miscible Gas Flood. *SPE 11130.*Exxon Production Research Company.

[4]. Lake, L. [1989] *Enhanced Oil Recovery*. Prentice Hall, Englewood Cliffs, NJ, specifically Chapter 11.

[5]. M.K. Jenkins. [1984] An Analytical Model for Water/Gas Miscible Displacements. *SPE/DOE 12632.*Exxon Production Research Co.

[6]. M. Namani, J. Kleppe. [2011] Investigation Of The Effect Of Some Parameters In Miscible WAG Process Using Black-Oil And Compositional Simulators. *SPE 143297*.NTNU.

[7]. MehranNamani, Jon kleppe, Lars Høier, HanssanKarimaie& Ole Torsæter. [2012] Analytical Model for Zones Distribution in Non-Horizontal Miscible WAG Injection. Energy and Environment Research 2(2): 159-168.

[8]. M. Namani, Lars Høier, and Jon Kleppe. [June2013] Advantages of Up-Dip Water-Miscible Gas Injection. *SPE 143297*.NTNU.

[9]. MehranNamani, YaserSouraki, Lars Høier, Hassan Karimaie, Jon Kleppe and Ole Torsæter. [2013] Experimental Study of Miscible Hot WAG Injection in Heavy Oil and Slightly Heavy Oil Reservoirs. International Journal of Petroleum Science and Technology 7(3): 265-278.

[10].W. R. Rossen, C. J. van Duijn.[2010] Gravity Segregation in Steady-State Horizontal Flow in Homogeneous Reservoirs. The University of Texas at Austin, and Eindhoven University of Technology.

[11].Sigurd íJ åkupsstovu, Dengen Zhou, JairamKamath, Lou Durlofsky, Erling H. Stenby. [May 2001] Upscaling of Miscible Displacement Process. IVC-SEP, Technical University of Denmark, Chevron Petroleum Technology Company, Stanford University, NTNU. Proceedings of the 6^{th} *Nordic Symposium on Petro-physics*, 15-16 May 2001.

Appendix A: Rock and fluid properties

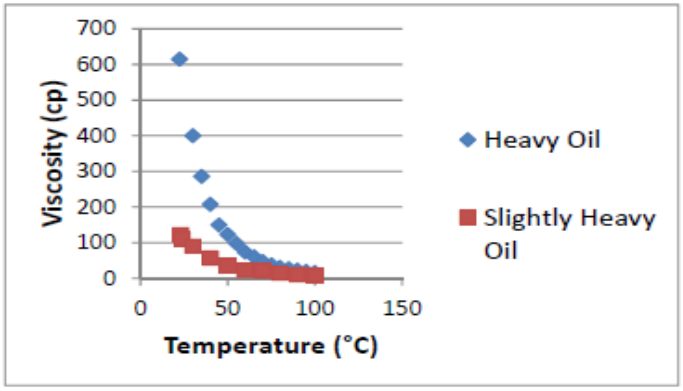

Figure A.1. Viscosity measurement of slightly heavy oil and heavy oil versus temperature (Namani *et al*, 2012).

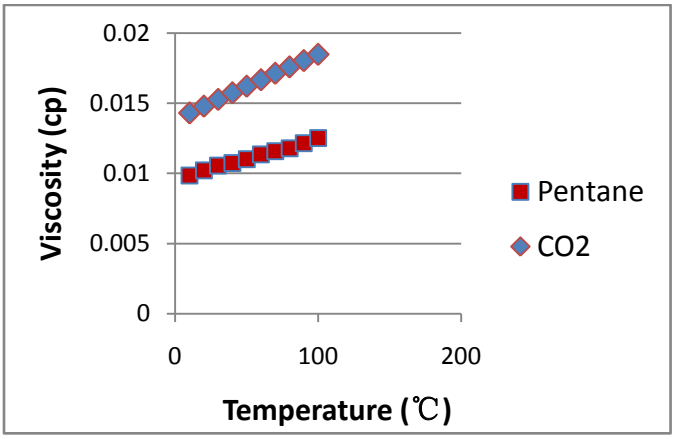

Figure A.2. Gas viscosity & Temperature.

Temp			Viscosity (cp)	
(°F)	(R)	(°C)	Pentane	CO_2
50	509	10	0.009857	0.014318
68	527	20	0.010217	0.014800
86	546	30	0.010574	0.015278
104	564	40	0.010754	0.015750
122	582	50	0.011011	0.016217
140	600	60	0.011371	0.016679
158	618	70	0.011580	0.017137
176	636	80	0.011806	0.017590
194	654	90	0.012166	0.018039

212	672	100	0.012526	0.018482

Table A.1. Viscosity of Pentane and CO_2 & Temperature.

Relative permeability of oil-water two phase flow

Water relative permeability

$$k_{rw} = k_{we}\left(\frac{S_w - S_{wr}}{1 - S_{wr} - S_{or}}\right)^{cw} \quad \textbf{Eq.[A.1]}$$

Oil relative permeability

$$k_{ro} = k_{oe}\left(\frac{1 - S_w - S_{or}}{1 - S_{wr} - S_{or}}\right)^{co} \quad \textbf{Eq.[A.2]}$$

Relative permeability of gas-water two phase flow

Water relative permeability

$$k_{rw} = k_{we}\left(\frac{S_w - S_{wr}}{1 - S_{wr} - S_{gr}}\right)^{cw} \quad \textbf{Eq.[A.3]}$$

Gas relative permeability

$$k_{rg} = k_{ge}\left(\frac{1 - S_w - S_{gr}}{1 - S_{wr} - S_{gr}}\right)^{cg} \quad \textbf{Eq.[A.4]}$$

$\mathbf{S_{wr}}$	0.05	$\mathbf{k_{we}}$	0.465	$\mathbf{C_w}$	2.98
$\mathbf{S_{or}}$	0.17	$\mathbf{k_{oe}}$	0.662	$\mathbf{C_o}$	3.44
$\mathbf{S_{gr}}$	0.17	$\mathbf{k_{ge}}$	0.662	$\mathbf{C_g}$	3.44

Table A.2. Constants for relative permeability curves.

Slightly Heavy Oil												
	φ (%)	$\mathbf{S_{wi}}$ **(%)**	**Volumetric heat capacity** $\mathbf{J/(m^3 \cdot ℃)}$			**Viscosity (cp)**					
						21.9 ℃			**100 ℃**		
			Water	**Oil**	**Sandstone**	μ_w	μ_o	μ_g	μ_w	μ_o	μ_g

			M_{tw}	M_{to}	M_{ts}			Pentane	CO_2			Pentane	CO_2
Hot WAG	33.9	10.99	4.20	1.8	2.15	4.0	124.4	0.011	0.015	4.0	15.0	0.0135	0.0185
Cold WAG	33.3	10.85											
Hot Water	34.8	10.99											
Heavy Oil													
	φ (%)	**S_{wi} (%)**	**Volumetric heat capacity $J/(m^3 \cdot ℃)$**			**Viscosity (cp)**							
						21.2 ℃				**100 ℃**			
			Water M_{tw}	**Oil M_{to}**	**Sandstone M_{ts}**	**μ_w**	**μ_o**	**μ_g**		**μ_w**	**μ_o**	**μ_g**	
								Pentane	**CO_2**			**Pentane**	**CO_2**
Hot WAG	33.6	7.59	4.20	2.1	2.15	4.0	651.7	0.010	0.015	4.0	20.0	0.0135	0.0185
Cold WAG	34.6	10.18											
Hot Water	33.0	8.68											

Table A.3. Rock and fluid properties in core-flooding experiments (Namani *et al*, 2013).

Reservoir & Fluid Properties		
Reservoir dimension	**160:1:25**	**[-]**
Reservoir Length	**3200**	**Ft**
Reservoir Width	**1500**	**ft**
Reservoir Thickness (isopach)	**500**	**ft**
Grid block size	$20 \times 20 \times 20$	ft^3
Porosity	**0.25**	**[-]**
Formation Permeability (X,Y,Z Directions)	**20**	**md**
Reference Depth	**4000**	**ft**

Initial Reservoir Pressure at reference depth	**4000**	**psia**
WAG ratio	**1:1**	**[-]**
Total Volumetric Injection Rate	**9000**	**RB/day**
Primary Production Rate	**9000**	**RB/day**
Initial Water Saturation	**0.2**	**[-]**
Water Density Surface Conditions	**62.4**	**lb/ft^3**
Water Formation Volume Factor at 4000 psia	**1.0**	**RB/STB**
Water Compressibility at 4000 psia	**3.3E-6**	**1/psi**
Water Viscosity at 4000 psia	**0.7**	**cp**
Oil Density at Surface Conditions	**38.53**	**lb/ft^3**
Oil Formation Volume Factor at 4000 psia	**1.30011**	**RB/STB**
Oil Viscosity at 4000 psia	**0.167**	**cp**
Gas Density at Surface Conditions	**0.06864**	**lb/ft^3**
Gas Formation Volume Factor at 4000 psia	**1.00022**	**RB/Mscf**
Gas Viscosity at 4000 psia	**0.034**	**cp**
Rock Compressibility at 4000 psia	**5E-6**	**1/psi**
Todd-Longstaff Mixing Parameter (base case)	**1.0**	**[-]**

Table A.4. Reservoir and fluid properties for numerical simulation (Namani *et al,* 2011).

Appendix B: Statistical data of segregation distance

Water-wet, $k_v = 20$ md, WAG=1:1							
q_t (RB/day)			10°	20°	30°	45°	60°
10^4	Up	$L_{h,dipping}$ (ft)	1140	1120	1030	940	760
		L_D	**0.9540**	**0.9372**	**0.8619**	**0.7866**	**0.6360**
	Down	$L_{h,dipping}$ (ft)	1480	1360	1380	1440	1420
		L_D	**1.2385**	**1.1381**	**1.1548**	**1.2050**	**1.1873**
	$L_{horizon}$ (ft)		1195	1195	1195	1195	1195
1.5×10^4	Up	$L_{h,dipping}$ (ft)	1660	1640	1500	1360	1200
		L_D	**0.9432**	**0.9318**	**0.8523**	**0.7727**	**0.6818**
	Down	$L_{h,dipping}$ (ft)	2140	1940	1920	1980	1920
		L_D	**1.2159**	**1.1023**	**1.0909**	**1.1250**	**1.0903**
	$L_{horizon}$ (ft)		1760	1760	1760	1760	1760
2×10^4	Up	$L_{h,dipping}$ (ft)	2160	2180	1980	1700	1620
		L_D	**0.9474**	**0.9561**	**0.8684**	**0.7456**	**0.7105**
	Down	$L_{h,dipping}$ (ft)	2740	2500	2460	2440	2340
		L_D	**1.2018**	**1.0965**	**1.0789**	**1.0702**	**1.0263**
	$L_{horizon}$ (ft)		2280	2280	2280	2280	2280

TableC.1. The effect of total volumetric injection rate on complete segregation distance $L_{g,dip}$.

Water-wet, $k_v = 25$ md, $q_t = 10000$ RB/day							
WAG (-)			**10°**	**20°**	**30°**	**45°**	**60°**
1:4	**Up**	$L_{h,dipping}$ (ft)	980	960	860	780	720
		L_D	**0.9800**	**0.9600**	**0.8600**	**0.7800**	**0.7200**
	Down	$L_{h,dipping}$ (ft)	1080	1140	1200	1200	1240
		L_D	**1.0800**	**1.1400**	**1.200**	**1.200**	**1.240**
	$L_{horizon}$ (ft)		1000	1000	1000	1000	1000
2:3	**Up**	$L_{h,dipping}$ (ft)	1420	1400	1240	1120	1000
		L_D	**0.9726**	**0.9589**	**0.8493**	**0.7671**	**0.6849**
	Down	$L_{h,dipping}$ (ft)	1580	1650	1660	1560	1700
		L_D	**1.0822**	**1.1301**	**1.1370**	**1.0685**	**1.1644**
	$L_{horizon}$ (ft)		1460	1460	1460	1460	1460
1:1	**Up**	$L_{h,dipping}$ (ft)	1620	1600	1480	1260	1200
		L_D	**0.9643**	**0.9524**	**0.8810**	**0.7500**	**0.7143**
	Down	$L_{h,dipping}$ (ft)	1840	1880	1820	1880	1840
		L_D	**1.0952**	**1.1190**	**1.0833**	**1.1190**	**1.0952**
	$L_{horizon}$ (ft)		1680	1680	1680	1680	1680

TableC.2. The effect of WAG ratio on complete segregation distance $L_{g,dip}$.

Water-wet, WAG = 1:1, q_t = 10000 RB/day							
k_v (md)			10°	20°	30°	45°	60°
25	Up	$L_{h,dipping}$ (ft)	1160	1120	1030	860	790
		L_D	**0.9707**	**0.9372**	**0.8619**	**0.7197**	**0.6611**
	Down	$L_{h,dipping}$ (ft)	1480	1360	1380	1440	1390
		L_D	**1.2385**	**1.1381**	**1.1548**	**1.2050**	**1.1632**
	$L_{horizon}$ (ft)		1195	1195	1195	1195	1195
15	Up	$L_{h,dipping}$ (ft)	1770	1710	1560	1340	1200
		L_D	**0.9833**	**0.9500**	**0.8667**	**0.7444**	**0.6667**
	Down	$L_{h,dipping}$ (ft)	1880	2000	1950	2000	1880
		L_D	**1.044**	**1.1111**	**1.0833**	**1.1111**	**1.0444**
	$L_{horizon}$ (ft)		1800	1800	1800	1800	1800
10	Up	$L_{h,dipping}$ (ft)	2460	2360	2170	1820	1700
		L_D	**0.9801**	**0.9402**	**0.8645**	**0.7251**	**0.6773**
	Down	$L_{h,dipping}$ (ft)	2600	2510	2600	2640	2400
		L_D	**1.0359**	**1.0000**	**1.0359**	**1.0518**	**0.9562**
	$L_{horizon}$ (ft)		2510	2510	2510	2510	2510

TableC.3. The effect of vertical permeability k_v on complete segregation distance $L_{g,dip}$.

Up-dip Injection, WAG = 1:1, q_t = 10000 RB/day							
k_v (md)			10°	20°	30°	45°	60°
25	Oil Wet	$L_{h,dipping}$ (ft)	1140	1120	1000	880	800
		L_D	**0.9661**	**0.9492**	**0.8475**	**0.7197**	**0.6780**
	$L_{horizon}$ (ft)		1180	1180	1180	1180	1180
	Water Wet	$L_{h,dipping}$ (ft)	1160	1120	1030	860	790
		L_D	**0.9707**	**0.9372**	**0.8619**	**0.7197**	**0.6611**
	$L_{horizon}$ (ft)		1195	1195	1195	1195	1195
15	Oil Wet	$L_{h,dipping}$ (ft)	1760	1700	1560	1400	1350
		L_D	**0.9778**	**0.9444**	**0.8667**	**0.7778**	**0.7500**
	$L_{horizon}$ (ft)		1800	1800	1800	1800	1800
	Water Wet	$L_{h,dipping}$ (ft)	1770	1710	1560	1340	1200
		L_D	**0.9833**	**0.9500**	**0.8667**	**0.7444**	**0.6667**
	$L_{horizon}$ (ft)		1800	1800	1800	1800	1800
10	Oil Wet	$L_{h,dipping}$ (ft)	2550	2430	2270	2000	2000
		L_D	**0.9884**	**0.9419**	**0.8798**	**0.7752**	**0.7752**
	$L_{horizon}$ (ft)		2580	2580	2580	2580	2580
	Water Wet	$L_{h,dipping}$ (ft)	2460	2360	2170	1820	1700
		L_D	**0.9801**	**0.9402**	**0.8645**	**0.7251**	**0.6773**
	$L_{horizon}$ (ft)		2510	2510	2510	2510	2510

TableC.4. The effect of phase relative permeability (combined with k_v) on complete segregation distance $L_{g,dip}$.